A concise enzyme cascade enables the manufacture of natural and halogenated protoberberine alkaloids

Li *et al.*

Supplementary Note 1. Chemical characterization data

(*S*)-1-(3-hydroxy-4-methoxybenzyl)-1,2,3,4-tetrahydroisoquinoline-6,7-diol ((*S*)-3a)

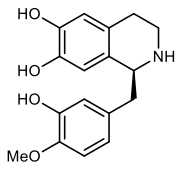

^{1}H NMR (600 MHz, DMSO-d_6) δ 9.17 (s, 1H), 8.98 (s, 1H), 8.92 (s, 1H), 8.62 (s, 1H), 6.89 (d, *J* = 8.2 Hz, 1H), 6.76 (d, *J* = 2.2 Hz, 1H), 6.69 (dd, *J* = 8.2, 2.1 Hz, 1H), 6.56 (s, 1H), 6.54 (s, 1H), 4.50 (t, *J* = 7.1 Hz, 1H), 3.76 (s, 3H), 3.35 – 3.30 (m, 1H), 3.14 (dd, *J* = 14.3, 6.0 Hz, 2H), 2.90 (dd, *J* = 14.4, 8.3 Hz, 1H), 2.85 (dt, *J* = 12.8, 6.5 Hz, 1H), 2.77 (dt, *J* = 16.8, 6.2 Hz, 1H) ppm.

^{13}C NMR (101 MHz, DMSO-d_6) δ 147.3, 147.0, 145.6, 144.5, 128.7, 123.2, 122.7, 120.6, 117.2, 115.6, 113.9, 112.8, 56.1, 55.7, 39.5, 24.8 ppm.

HRMS (ESI) calcd. $[C_{17}H_{19}NO_4+H]^+$ for 302.1378, 302.1372 (found).

(*S*)-1-(3-hydroxy-4-methoxybenzyl)-6-methoxy-1,2,3,4-tetrahydroisoquinolin-7-ol ((*S*)-4a)

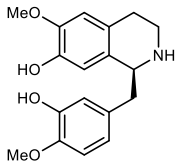

^{1}H NMR (400 MHz, Methanol-d_4) δ 6.95 (d, *J* = 8.2 Hz, 1H), 6.81 (d, *J* = 2.1 Hz, 1H), 6.80 (s, 1H), 6.76 (dd, *J* = 8.2, 2.2 Hz, 1H), 6.69 (s, 1H), 4.63 (dd, *J* = 9.0, 5.5 Hz, 1H), 3.88 (s, 3H), 3.87 (s, 3H), 3.54 – 3.46 (m, 1H), 3.38 (dd, *J* = 14.6, 5.5 Hz, 1H), 3.28 (dd, *J* = 12.8, 7.1 Hz, 1H), 3.13 – 3.04 (m, 1H), 3.01 (dd, *J* = 11.8, 5.5 Hz, 1H), 2.98 – 2.91 (m, 1H) ppm.

^{13}C NMR (101 MHz, Methanol-d_4) δ 147.9, 147.4, 146.9, 145.5, 127.7, 123.6, 122.2, 120.4, 115.9, 112.7, 111.8, 111.2, 56.4, 55.0, 55.0, 39.5, 39.2, 24.5 ppm.

HRMS (ESI) calcd. $[C_{18}H_{21}NO_4+H]^+$ for 316.1543, 316.1544 (found).

(*S*)-1-(3-hydroxy-4-methoxybenzyl)-6-methoxy-2-methyl-1,2,3,4-tetrahydroisoquinolin-7-ol ((*S*)-5a)[1]

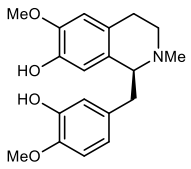

^{1}H NMR (400 MHz, Chloroform-*d*) δ 6.73 (dd, *J* = 5.1, 3.1 Hz, 2H), 6.60 (dd, *J* = 8.2, 2.1 Hz, 1H), 6.55 (s, 1H), 6.31 (s, 1H), 5.90 (br, 2H), 3.85 (s, 3H), 3.85 (s, 3H), 3.78 (t, *J* = 6.3 Hz, 1H), 3.31 – 3.22 (m, 1H), 3.18 (dd, *J* = 13.8, 5.2 Hz, 1H), 2.90 – 2.78 (m, 3H), 2.72 – 2.64 (m, 1H), 2.53 (s, 3H) ppm.

HRMS (ESI) calcd. $[C_{19}H_{23}NO_4+H]^+$ for 330.1700, 330.1707 (found).

(*S*)-3,10-dimethoxy-5,8,13,13a-tetrahydro-6H-isoquinolino[3,2-a] isoquinoline-2,9-diol ((*S*)-6a)[2]

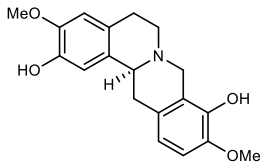

^{1}H NMR (600 MHz, Chloroform-*d*) δ 6.83 (s, 1H), 6.73 (d, *J* = 8.2 Hz, 1H), 6.67 (d, *J* = 8.2 Hz, 1H), 6.60 (s, 1H), 5.66 (s, 1H), 5.49 (s, 1H), 4.24 (d, *J* = 15.4 Hz, 1H), 3.88 (s, 3H), 3.87 (s, 3H), 3.58 – 3.48 (m, 2H), 3.27 – 3.12 (m, 3H), 2.82 (t, *J* = 13.7 Hz, 1H), 2.69 – 2.62 (m, 2H) ppm.

HRMS (ESI) calcd. $[C_{19}H_{21}NO_4+H]^+$ for 328.1543, 328.1523 (found).

(*S*)-2,3,9,10-tetramethoxy-5,8,13,13a-tetrahydro-6H-isoquinolino[3,2-a] isoquinoline ((*S*)-8a)[3]

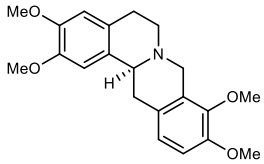

^{1}H NMR (600 MHz, Chloroform-*d*) δ 6.88 (d, *J* = 8.3 Hz, 1H), 6.79 (d, *J* = 8.3 Hz, 1H), 6.74 (s, 1H), 6.62 (s, 1H), 4.25 (d, *J* = 15.7 Hz, 1H), 3.89 (s, 3H), 3.87 (s, 3H), 3.86 (s, 3H), 3.85 (s, 3H), 3.58 – 3.52 (m, 2H), 3.27 (dd, *J* = 15.8, 3.8 Hz, 1H), 3.24 – 3.18 (m, 1H), 3.18 – 3.12 (m, 1H), 2.84 (dd, *J* = 15.8, 11.3 Hz, 1H), 2.70 – 2.62 (m, 2H) ppm.

HRMS (ESI) calcd. $[C_{21}H_{25}NO_4+H]^+$ for 356.1856, 356.1852 (found).

2-(4-chloro-3-hydroxyphenyl) acetic acid (1b)

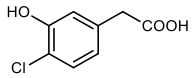

^{1}H NMR (400 MHz, DMSO-*d*6) δ 12.34 (s, 1H), 10.10 (s, 1H), 7.24 (d, *J* = 8.1 Hz, 1H), 6.88 (d, *J* = 2.0 Hz, 1H), 6.69 (dd, *J* = 8.2, 2.0 Hz, 1H), 3.48 (s, 2H) ppm.

2-(3-chloro-5-hydroxyphenyl) acetic acid (1c)

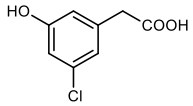

^{1}H NMR (400 MHz, DMSO-d_6) δ 12.37 (s, 1H), 9.86 (s, 1H), 6.75 (t, *J* = 1.7 Hz, 1H), 6.69 (t, *J* = 2.1 Hz, 1H), 6.64 (t, *J* = 1.8 Hz, 1H), 3.50 (s, 2H). ppm.

2-(2-chloro-5-hydroxyphenyl) acetic acid (1d)

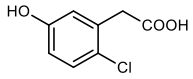

^{1}H NMR (600 MHz, DMSO-d_6) δ 12.42 (s, 1H), 9.66 (s, 1H), 7.19 (d, *J* = 8.6 Hz, 1H), 6.78 (s, 1H), 6.68 (d, *J* = 8.4 Hz, 1H), 3.59 (s, 2H) ppm.

2-(4-fluoro-3-hydroxyphenyl) acetic acid (1e)

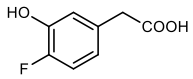

^{1}H NMR (400 MHz, DMSO-d_6) δ 12.28 (s, 1H), 9.77 (s, 1H), 7.04 (dd, *J* = 11.4, 8.3 Hz, 1H), 6.86 (dd, *J* = 8.6, 2.2 Hz, 1H), 6.65 (m, *J* = 8.4, 4.3, 2.2 Hz, 1H), 3.46 (s, 2H) ppm.

2-(3-fluoro-5-hydroxyphenyl) acetic acid (1f)

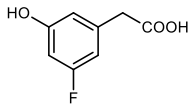

^{1}H NMR (400 MHz, DMSO-d_6) δ 12.36 (s, 1H), 9.84 (s, 1H), 6.51 (dd, *J* = 9.1, 2.0 Hz, 2H), 6.44 (dt, *J* = 10.9, 2.3 Hz, 1H), 3.49 (s, 2H)) ppm.

2-(2-fluoro-5-hydroxyphenyl) acetic acid (1g)

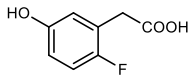

^{1}H NMR (400 MHz, DMSO-d_6) δ 12.39 (s, 1H), 9.31 (s, 1H), 6.95 (t, J = 9.2 Hz, 1H), 6.69 (dd, J = 6.3, 3.0 Hz, 1H), 6.64 (dt, J = 8.8, 3.7 Hz, 1H), 3.51 (d, J = 1.5 Hz, 2H) ppm.

(*S*)-10-chloro-2,3,9-trimethoxy-5,8,13,13a-tetrahydro-6H-isoquinolino[3,2-a] isoquinoline ((*S*)-8b)

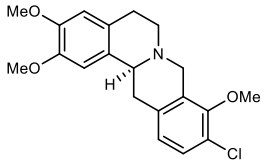

^{1}H NMR (600 MHz, Chloroform-*d*) δ 7.12 (d, J = 8.0 Hz, 1H), 6.82 (d, J = 8.1 Hz, 1H), 6.65 (s, 1H), 6.56 (s, 1H), 4.17 (d, J = 15.8 Hz, 1H), 3.82 (s, 3H), 3.81 (s, 6H), 3.51 (d, J = 14.3 Hz, 2H), 3.22 (d, J = 16.2 Hz, 1H), 3.14 (d, J = 11.4 Hz, 1H), 3.08 (t, J = 13.9 Hz, 1H), 2.79 (t, J = 13.9 Hz, 1H), 2.61 (t, J = 12.8 Hz, 2H) ppm.

HRMS (ESI) calcd. $[C_{20}H_{22}ClNO_3+H]^+$ for 360.1361, 360.1331 (found).

Supplementary Table 1. The calculation of the interaction energy between (*S*)-5a and 4 Å protein residues of *Ec*BBE (including FAD).

	The calculation of the interaction energy between (*S*)-5a and 4 Å protein residues of *Ec*BBE (including FAD) (kcal/mol)
*Ec*BBE^{WT}	-55.09878
*Ec*BBE#	-67.42688

Supplementary Table 2. The calculation of the interaction energy between (*S*)-7a and 4 Å protein residues of *Tf*S9OMT (including SAM).

	The calculation of the interaction energy between (*S*)-7a and 4 Å protein residues of *Tf*S9OMT (including SAM) (kcal/mol)
*Tf*S9OMT^{M} with (*S*)-**7a**	-50.62176
*Tf*S9OMT# with (*S*)-**7a**	-52.71836

Supplementary Table 3. The volume of substrate-binding pocket of *Tf*S9OMT.

	The volume of substrate-binding pocket (Å^3)
*Tf*S9OMT^{M}	647
*Tf*S9OMT#	668

Supplementary Table 4. The information of the regents used in this study.

Regents	Purity (%)	Source
Primers		Exsyn-bio (Wuxi, China)
DNA marker		TaKaRa
Protein marker		TaKaRa
PrimerSTAR MAX DNA Polymerase		TaKaRa
2 × Phanta Flash Master Mix		Vazyme
Tryptone		OXOID
Yeast extract		OXOID
NaCl	99.8	China National Pharmaceutical Group Corp (Shanghai, China)
Acetonitrile (HPLC)	99.9	Adamas-Beta (Shanghai, China)
Methanol (HPLC)	99.9	Adamas-Beta (Shanghai, China)
2-(3-hydroxy-4-methoxyphenyl) acetic acid (**1a**)	98	Energy Chemical (Shanghai, China)
Dopamine hydrochloride	98	Energy Chemical (Shanghai, China)
L-Ascorbic Acid Sodium Salt	98	Energy Chemical (Shanghai, China)
Adenosine5'-(tetrahydrogen triphosphate), disodiuM salt, trihydrate (9CI)	97	Energy Chemical (Shanghai, China)
L-Methionine	98	Energy Chemical (Shanghai, China)
Flavin adenine dinucleotide dis odium salt dihydrate	98	Bide Pharmatech (Shanghai, China)

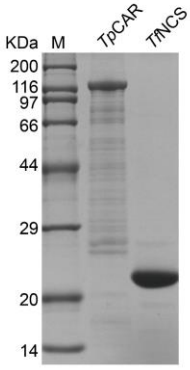

Supplementary Figure 1. SDS-PAGE analysis of purified *Tp*CAR and *Tf*NCS. M: marker; lane 1: *Tp*CAR; lane 2: *Tf*NCS. Source data are provided as a Source Data file.

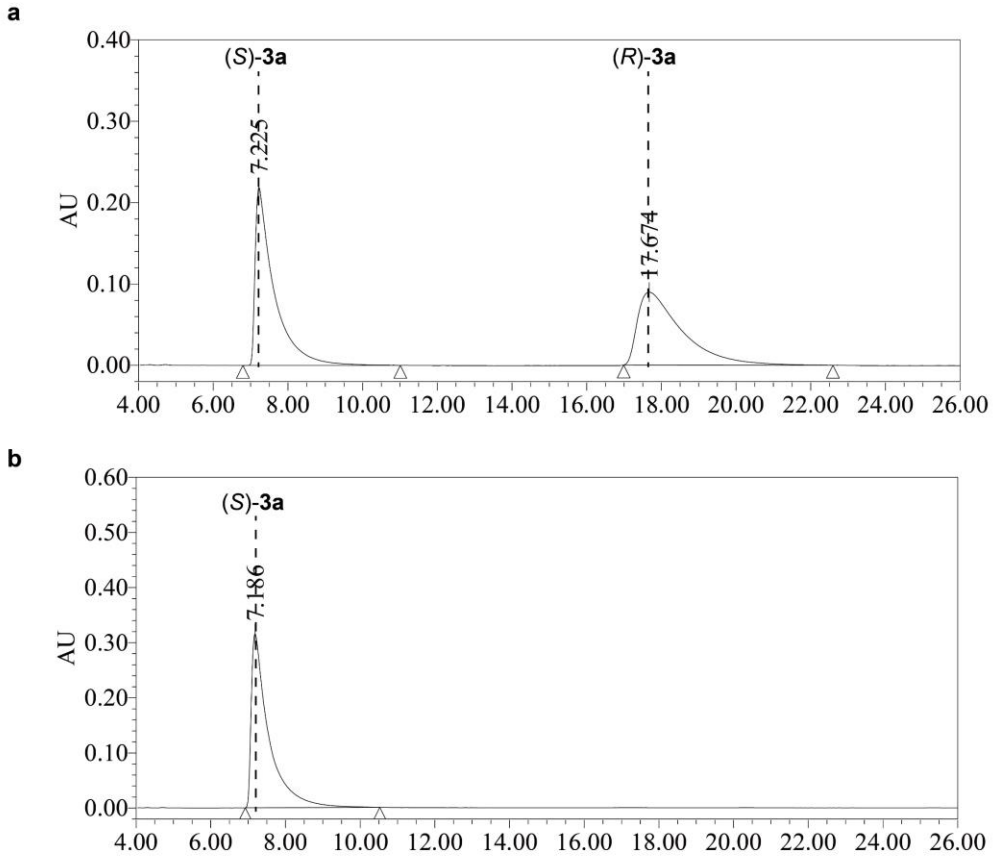

Supplementary Figure 2. Enantioselectivity analysis of *Tf*NCS. a Chiral HPLC analysis of (*rac*)-**3a** synthesized by *Tp*CAR. Peak 1 (Retention time: 7.225 min, Area%: 50.79%), Peak 2 (Retention time: 17.674 min, Area%: 49.21%). **b** Chiral HPLC analysis of (*S*)-**3a** synthesized by *Tp*CAR and *Tf*NCS. Peak 1 (Retention time: 7.186 min, Area%: 100%). The enantioselectivities were analyzed via HPLC on a chiral stationary phase. HPLC: Chiral Pak® CHIRALCEL OD-H, n-hexane/isopropanol/diethylamine 75/25/0.1, flow rate = 1.2 mL/min, uv-vis λ =280 nm, t_{R1} = 7.2 min.

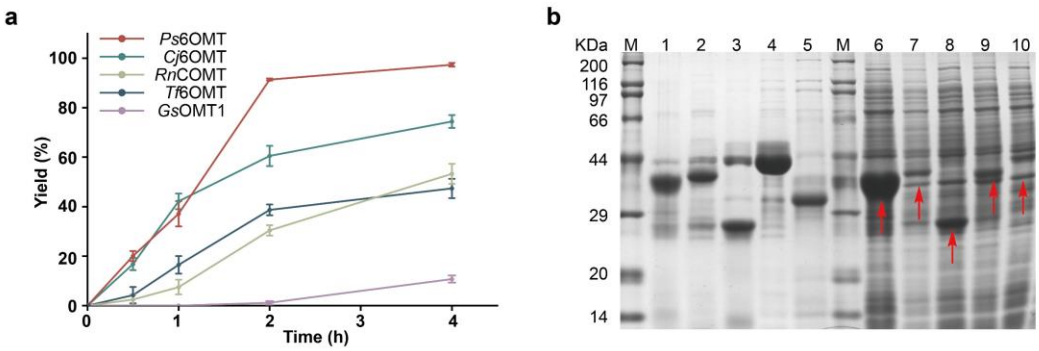

Supplementary Figure 3. Catalytic activity analysis and expression level of 6OMTs. a Time course of yields for transforming (*S*)-**3a** to (*S*)-**4a** by 6OMTs. **b** SDS-PAGE analysis of 6OMTs in *E. coli* BL21 (DE3). M: marker; lane 1: *Ps*6OMT; lane 2: *Tf*6OMT; lane 3: *Rn*COMT; lane 4: *Gs*OMT1; lane 5: *Cj*6OMT; lane 6: the supernatant of cell lysates expressing *Ps*6OMT; lane 7: the supernatant of cell lysates expressing *Tf*6OMT; lane 8: the supernatant of cell lysates expressing *Rn*COMT; lane 9: the supernatant of cell lysates expressing *Gs*OMT1; lane 10: the supernatant of cell lysates expressing *Cj*6OMT. All data is presented as mean value of three independent experiments and the error bars indicate ± sd. Source data are provided as a Source Data file.

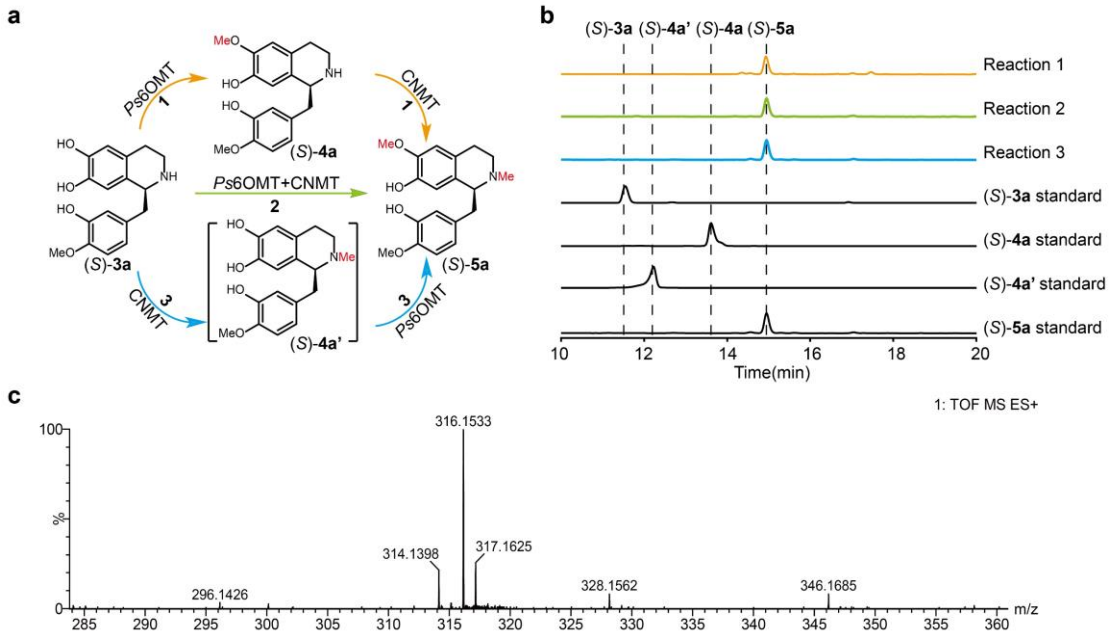

Supplementary Figure 4. Reaction sequence investigation of *Ps*6OMT and CNMT for the substrate (*S*)-3a and HRMS spectrum of (*S*)-4a'. a Three proposed reaction sequences from (*S*)-**3a** to (*S*)-**5a**. Reaction 1: (*S*)-**3a** was first *O*-methylated by *Ps*6OMT for 4 h, and then *N*-methylated by CNMT for 4 h. Reaction 2: (*S*)-**3a** was *O*-methylated and *N*-methylated simultaneously in the presence of both *Ps*6OMT and CNMT for 8 h. Reaction 3: (*S*)-**3a** was first *N*-methylated by CNMT for 4 h, and then *O*-methylated by *Ps*6OMT for 4 h. Reaction 1 is highlighted in orange, Reaction 2 is highlighted in green, and Reaction 3 is highlighted in blue. **b** HPLC analysis of (*S*)-**3a**, (*S*)-**4a,** (*S*)-**4a'** and (*S*)-**5a** in cascade reactions. Method for reaction 1: 5 μM *Ps*6OMT, 2 mM (*S*)-**3a**, 10 mM $MgCl_2$ and 4 mM SAM were incubated in a 200 μL reaction system for 4 h at 30 ℃. Next, the above reaction solution was boiled at 95 ℃ for 5 min and centrifuged at 20000 *g* for 5 min. Then, 5 μM CNMT was added into the above supernatant to initiate the reaction for 4 h at 30 ℃. Method for reaction 2: 5 μM *Ps*6OMT and 5 μM CNMT, 2 mM (*S*)-**3a**, 10 mM $MgCl_2$ and 4 mM SAM were simultaneously incubated in a 200 μL reaction system for 8 h at 30 ℃. Method for reaction 3: 5 μM *Ps*6OMT, 2 mM (*S*)-**3a**, 10 mM $MgCl_2$ and 4 mM SAM were incubated in a 200 μL reaction system for 4 h at 30 ℃. Next, the above reaction solution was boiled at 95 ℃ for 5 min and centrifuged at 20000 *g* for 5 min. Then, 5 μM CNMT was added into the above supernatant to initiate the reaction for 4 h at 30 ℃. **c** The HRMS spectrum (positive) showed *m/z* 316.1533 for $[M+H]^+$ (calcd. for $C_{18}H_{21}NO_4^+$, 316.1543). Source data are provided as a Source Data file.

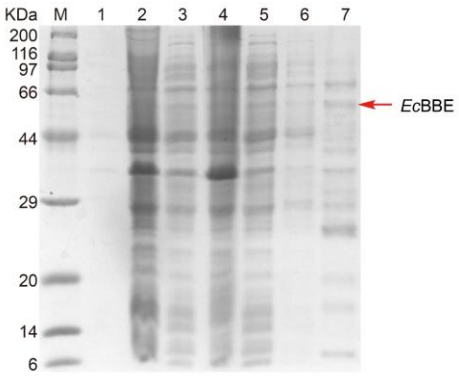

Supplementary Figure 5. SDS-PAGE analysis of *Ec*BBE expressed in *E. coli* BL21 (DE3). M: marker; lane 1: no IPTG induction; lane 2: cell lysates expressing *Ec*BBE; lane 3: the supernatant of cell lysates expressing *Ec*BBE; lane 4: the pellet of cell lysates; lane 5: flow through of crude enzyme; lane 6: washing fraction; lane 7: purified *Ec*BBE. Source data are provided as a Source Data file.

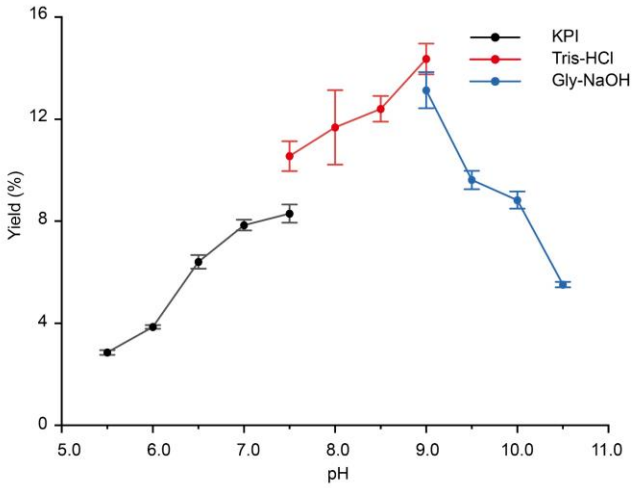

Supplementary Figure 6. Optimization of pH for *Ec*BBE. The buffers were potassium phosphate buffer (pH 5.5−7.5, 50 mM), Tris-HCl buffer (pH 7.5−9.0, 50 mM) and Glycine-NaOH (pH 9.0−10.0, 50 mM). All data is presented as mean value of three independent experiments and the error bars indicate ± sd. Source data are provided as a Source Data file.

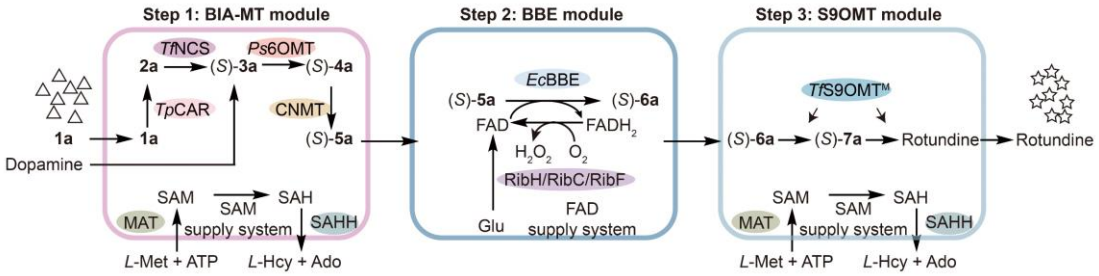

Supplementary Figure 7. Scheme of the designed biosynthetic pathway for Rotundine though one-pot three-step process. Three strains expressing enzymes of the BIA-MT, *Ec*BBE, and *Tf*S9OMT^{M} modules were constructed. (*S*)-**5a** was produced from **1a** and dopamine catalyzed by the strain containing the BIA-MT module with *L*-Met and ATP adding exogenously, and (*S*)-**6a** was produced from the supernatant of step 1 catalyzed by the strain containing *Ec*BBE. Rotundine was ultimately produced from the supernatant of step 2 catalyzed by the strain containing *Tf*S9OMT^{M} with *L*-Met and ATP adding exogenously.

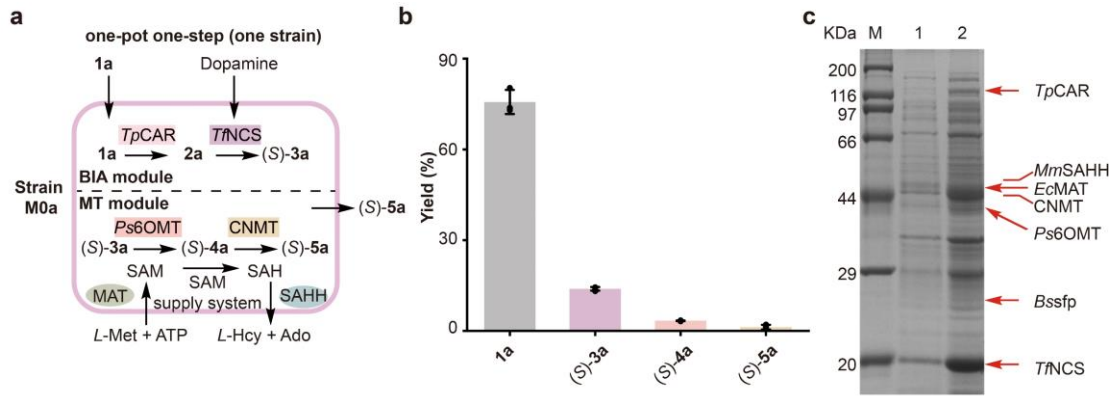

Supplementary Figure 8. Biosynthetic pathway toward (*S*)-5a from 1a and dopamine though one-pot one-step process. a Scheme of the designed biosynthetic pathway in strain M0a. One strain expressing enzymes of the BIA and MT modules was constructed. **b** Yields of (*S*)-**3a**, (*S*)-**4a** and (*S*)-**5a** in strain M0a corresponds to a theoretical yield of **1a**. The unconverted **1a** was also shown. **c** SDS-PAGE analysis of *Tp*CAR, *Bs*sfp, *Tf*NCS, *Ps*6OMT, CNMT, *Mm*SAHH and *Ec*MAT expressed in strain M0a, M: marker; lane 1: no IPTG induction; lane 2: cell lysates of strain M0a. All data is presented as mean value of three independent experiments and the error bars indicate ± sd. Source data are provided as a Source Data file.

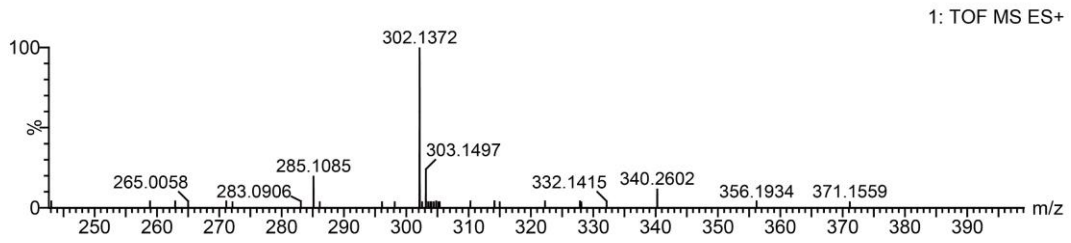

Supplementary Figure 9. HRMS spectrum of (*S*)-3a. The HRMS spectrum (positive) showed *m/z* 302.1372 for $[M+H]^+$ (calcd. for $C_{17}H_{19}NO_4^+$, 302.1378).

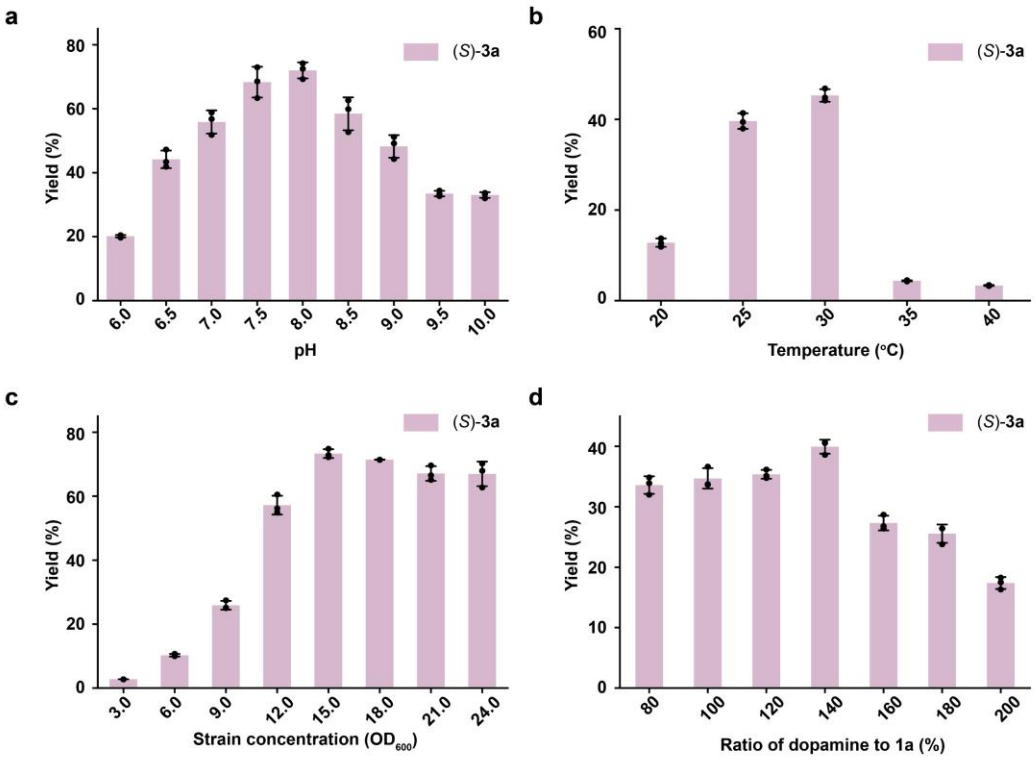

Supplementary Figure 10. Optimization of the parameters to improve the yield of (*S*)-3a. **a** Optimization of the reaction pH in BIA module by strain M1d. **b** Optimization of the reaction temperature in the BIA module by strain M1d. **c** Optimization of the concentration of the strain M1d in the BIA module. **d** Optimization of the ratio of dopamine to **1a** in the BIA module by strain M1d. The yields correspond to a theoretical yield of **1a** in the BIA module. All data is presented as mean value of three independent experiments and the error bars indicate ± sd. Source data are provided as a Source Data file.

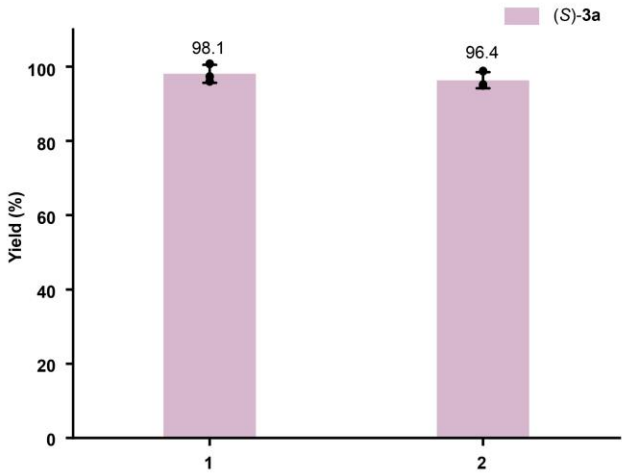

Supplementary Figure 11. Yields of (*S*)-3a in the reaction mixture and the supernatant of the reaction mixture. 1: the reaction mixture; 2: the supernatant of the reaction mixture. All data is presented as mean value of three independent experiments and the error bars indicate ± sd. Source data are provided as a Source Data file.

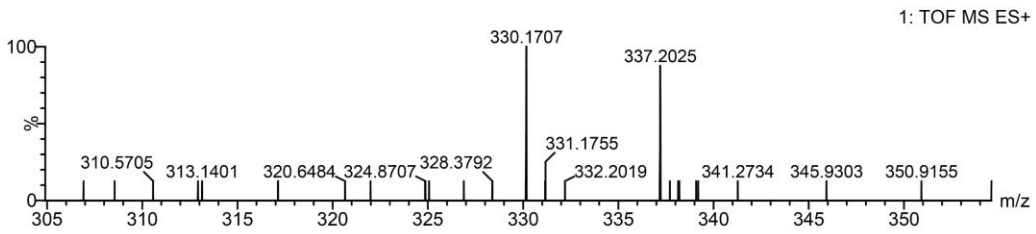

Supplementary Figure 12. HRMS spectrum of (*S*)-5a. The HRMS spectrum (positive) showed *m/z* 330.1707 for $[M+H]^+$ (calcd. for $C_{19}H_{23}NO_4^+$, 330.1700).

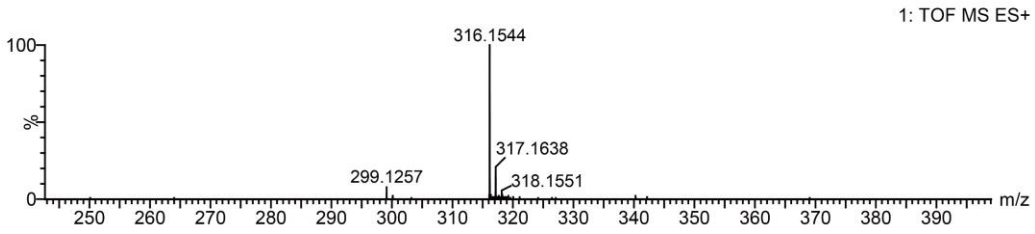

Supplementary Figure 13. HRMS spectrum of (*S*)-4a. The HRMS spectrum (positive) showed *m/z* 316.1544 for $[M+H]^+$ (calcd. for $C_{18}H_{21}NO_4^+$, 316.1543).

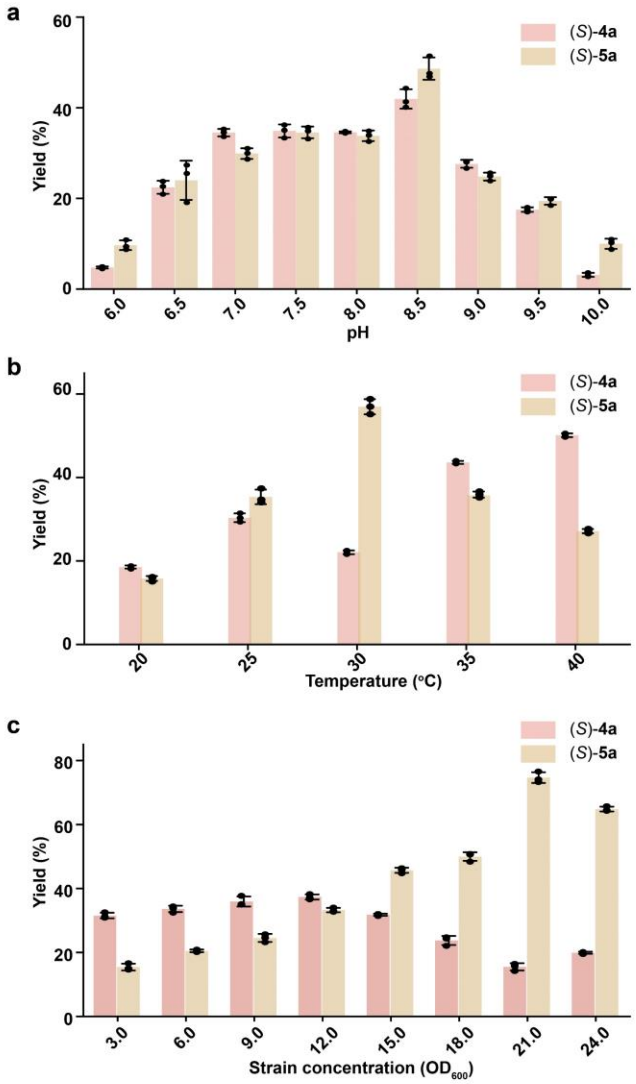

Supplementary Figure 14. Optimization of the parameters to improve the yield of (*S*)-4a and (*S*)-5a correspond to a theoretical yield of 1a in the MT module. a Optimization of the reaction pH in the MT module by strain M2c. **b** Optimization of the reaction temperature in the MT module by strain M2c. **c** Optimization of the concentration of strain M2c in the MT module. All data is presented as mean value of three independent experiments and the error bars indicate ± sd. Source data are provided as a Source Data file.

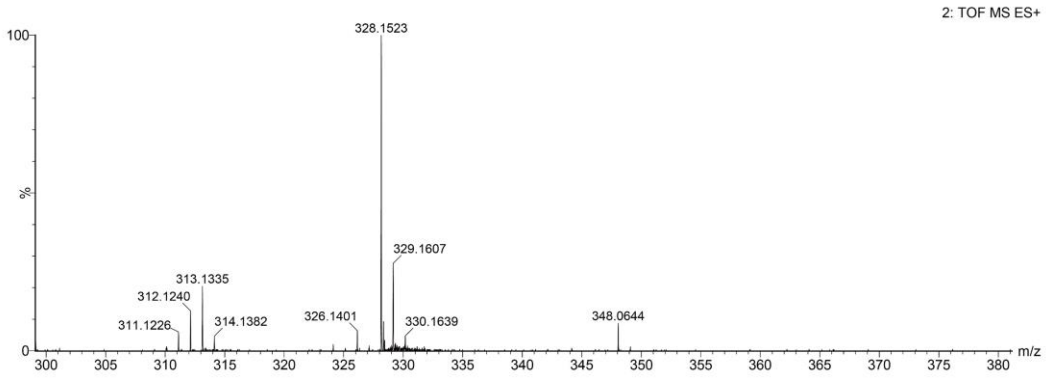

Supplementary Figure 15. HRMS spectrum of (*S*)-6a. The HRMS spectrum (positive) showed *m/z* 328.1543 for $[M+H]^+$ (calcd. for $C_{19}H_{21}NO_4^+$, 328.1523).

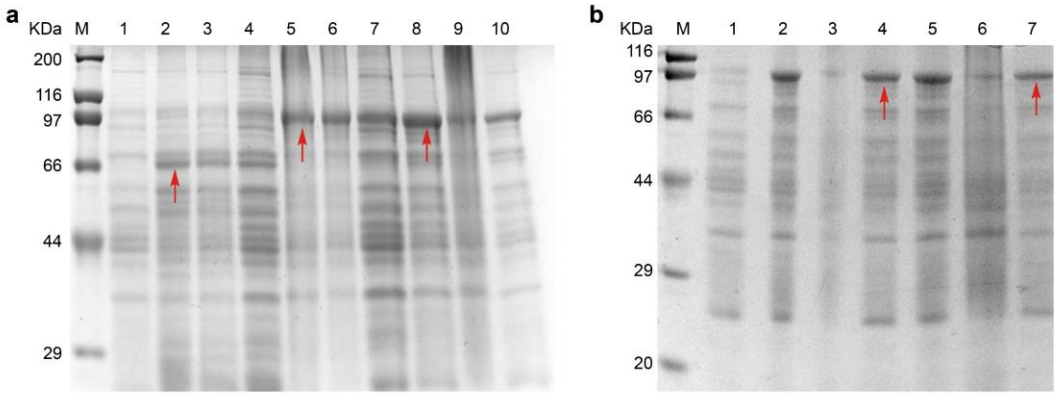

Supplementary Figure 16. SDS-PAGE analysis of *Ec*BBE with *N*-terminal signal peptide truncation and a solubilizing tag (MBP) expressed in *E. coli* BL21 (DE3). a M: marker; lane 1: no IPTG induction; lane 2: cell lysates expressing *Ec*BBE using vector pet21b; lane 3: the pellet of cell lysates expressing *Ec*BBE using vector pet21b; lane 4: the supernatant of cell lysates expressing *Ec*BBE using vector pet21b; lane 5: cell lysates expressing *Ec*BBE with *N*-terminal signal peptide truncation and a solubilizing tag (MBP) using vector pet21b; lane 6: the pellet of cell lysates expressing *Ec*BBE with *N*-terminal signal peptide truncation and a solubilizing tag (MBP) using vector pet21b; lane 7: the supernatant of cell lysates expressing *Ec*BBE with *N*-terminal signal peptide truncation and a solubilizing tag (MBP) using vector pet21b; lane 8: cell lysates expressing *Ec*BBE with *N*-terminal signal peptide truncation and a solubilizing tag (MBP) using vector pCDFDuet in M3d; lane 9: the pellet of cell lysates expressing *Ec*BBE with *N*-terminal signal peptide truncation and a solubilizing tag (MBP) using vector pCDFDuet in M3d; lane 10: the supernatant of cell lysates expressing *Ec*BBE with *N*-terminal signal peptide truncation and a solubilizing tag (MBP) using vector pCDFDuet in M3d. Target proteins in the cell lysates are indicated by red arrows. **b** M: marker; lane 1: no IPTG induction; lane 2: cell lysates of M3g; lane 3: the pellet of cell lysates of M3g; lane 4: the supernatant of cell lysates of M3g; lane 5: cell lysates of M3d; lane 6: the pellet of cell lysates of M3d; lane 7: the supernatant of cell lysates of M3d. Target proteins in the supernatant are indicated by red arrows. Source data are provided as a Source Data file.

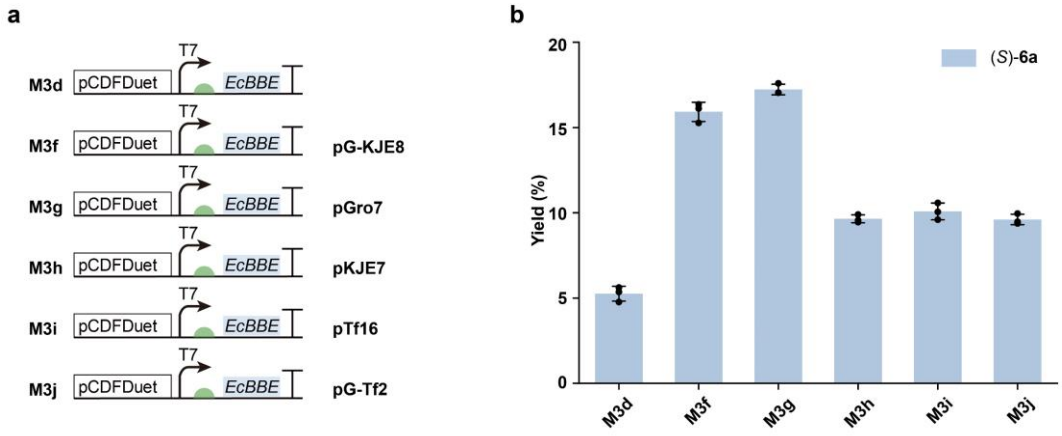

Supplementary Figure 17. Optimization of molecular chaperones to improve the yield of (*S*)-6a. a Construction of five engineered strains containing different molecular chaperones. **b** Yields of (*S*)-**6a** correspond to a theoretical yield of **1a** using strain M3d, M3f, M3g, M3h, M3i and M3j. All data is presented as mean value of three independent experiments and the error bars indicate ± sd. Source data are provided as a Source Data file.

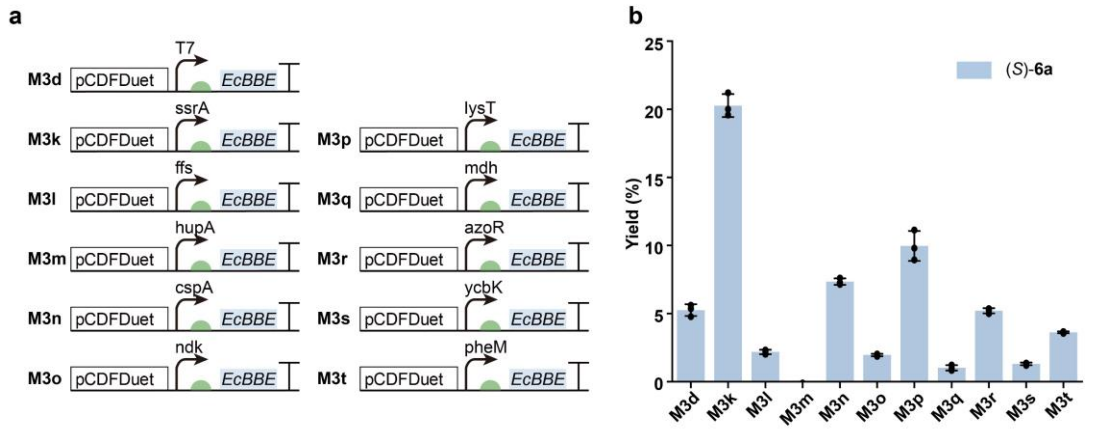

Supplementary Figure 18. Optimization of ten promoters from the constitutive promoter library to improve the yield of (*S*)-6a. a Construction of ten engineered strains containing different promoters. **b** Yields of (*S*)-**6a** correspond to a theoretical yield of **1a** using strain M3d, M3k, M3l, M3m, M3n, M3o, M3p, M3q, M3r, M3s and M3t. All data is presented as mean value of three independent experiments and the error bars indicate ± sd. Source data are provided as a Source Data file.

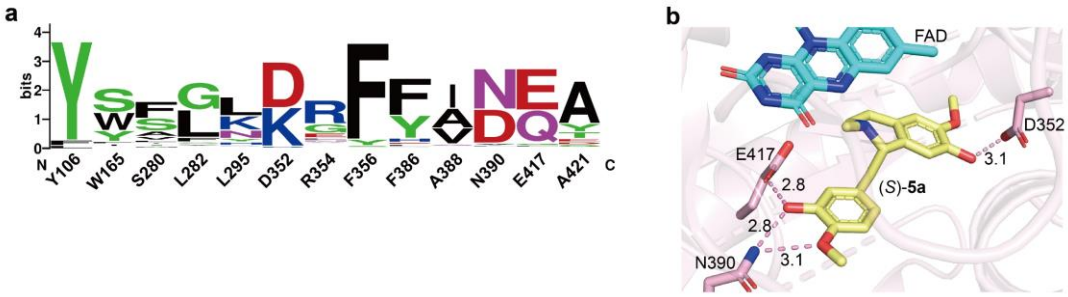

Supplementary Figure 19. Analysis of residues of *Ec*BBE within 4.0 Å surrounding (*S*)-5a. a Amino acid sequence conservation analysis. A total of 100 sequences exhibiting at least 50% identity with *Ec*BBE were generated using BLAST tools available through NCBI. Sequence alignment was conducted using BioEdit, and the regions of interest were visualized using WebLogo. **b** Hydrogen bonds between (*S*)-**5a** and *Ec*BBE.

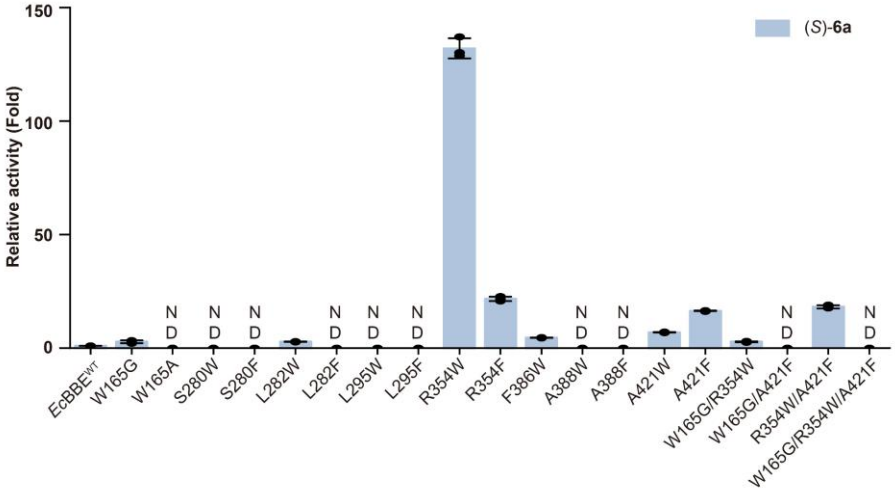

Supplementary Figure 20. Relative activity of all mutants of *Ec*BBE^{WT} toward (*S*)-5a *in vitro*. The relative activity is defined as the ratio of the (*S*)-**6a** titer of *Ec*BBE^{WT} mutants to that of *Ec*BBE^{WT}. ND: not detected. All data is presented as mean value of three independent experiments and the error bars indicate ± sd. Source data are provided as a Source Data file.

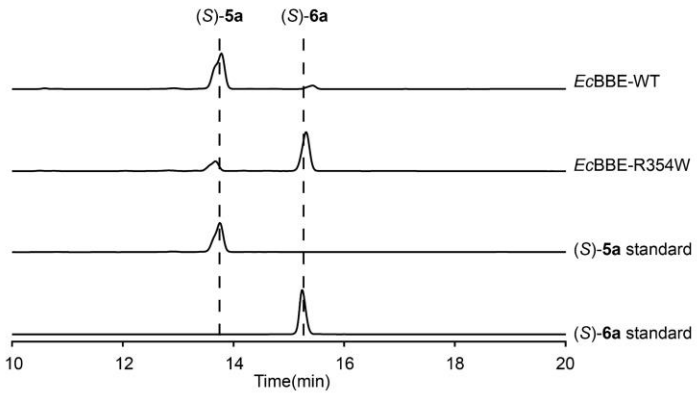

Supplementary Figure 21. HPLC analysis of *Ec*BBE and its mutants. Source data are provided as a Source Data file.

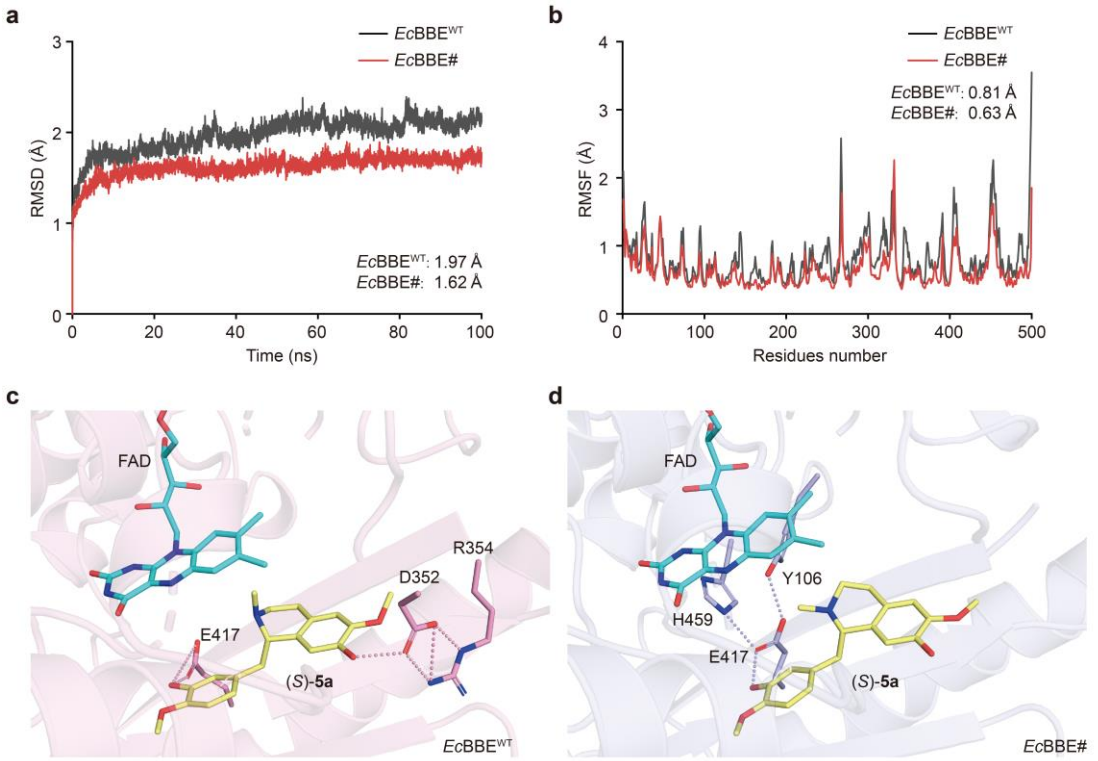

Supplementary Figure 22. Molecular dynamics simulation analysis and representative snapshot for wild type *Ec*BBE and mutant *Ec*BBE#. a Root mean square deviation (RMSD). **b** Root mean square fluctuation (RMSF). **c** The representative snapshot of *Ec*BBE^{WT}. **d** The representative snapshot of *Ec*BBE#. Light pink or light blue dotted lines: hydrogen-bonds. Source data are provided as a Source Data file.

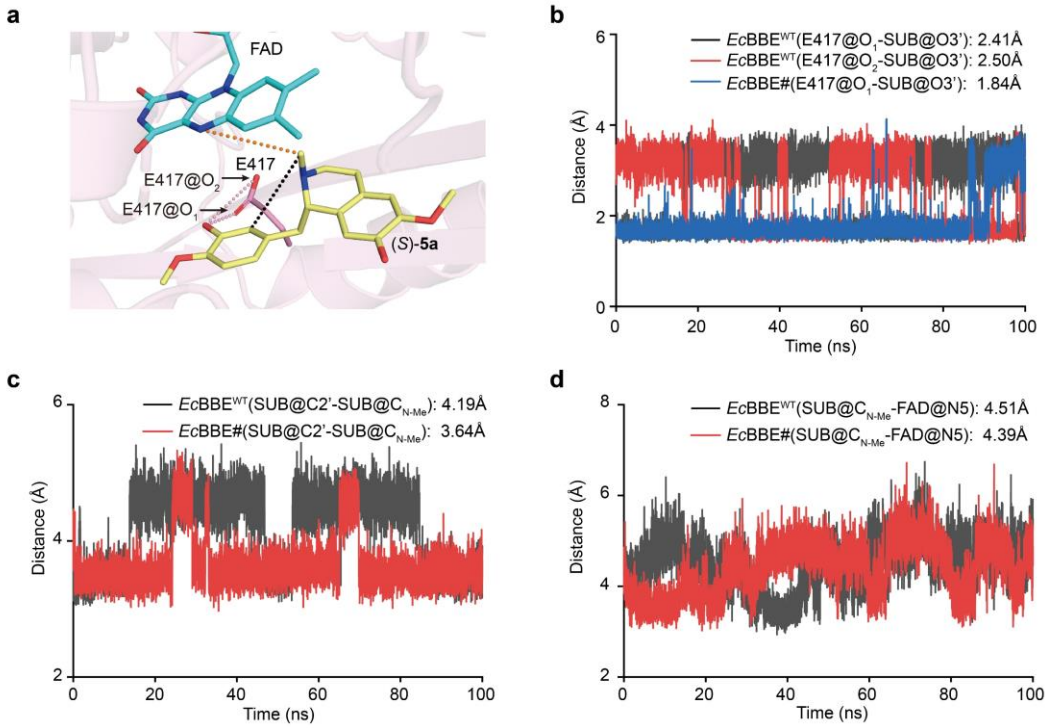

Supplementary Figure 23. Important distance investigations of *Ec*BBE^{WT} or *Ec*BBE# in MD simulations. a Schematic representation of the three interatomic distances. Light pink dotted lines: the distance between the C3′ OH group of (*S*)-**5a** and two oxygen atoms in the carboxyl group of E417 in *Ec*BBE; Black dotted lines: the distance between the C2′ carbon and the carbon atom on the *N*-methyl group of (*S*)-**5a**; Orange dotted lines: the distance between the carbon atom on the *N*-methyl group of (*S*)-**5a** and N5 atom of FAD. **b** The distance between the C3′ OH group of (*S*)-**5a** and two oxygen atoms in the carboxyl group of E417 in *Ec*BBE. **c** The distance between the C2′ carbon and the carbon atom on the *N*-methyl group of (*S*)-**5a**. **d** The distance between the carbon atom on the *N*-methyl group of (*S*)-**5a** and N5 atom of FAD. Source data are provided as a Source Data file.

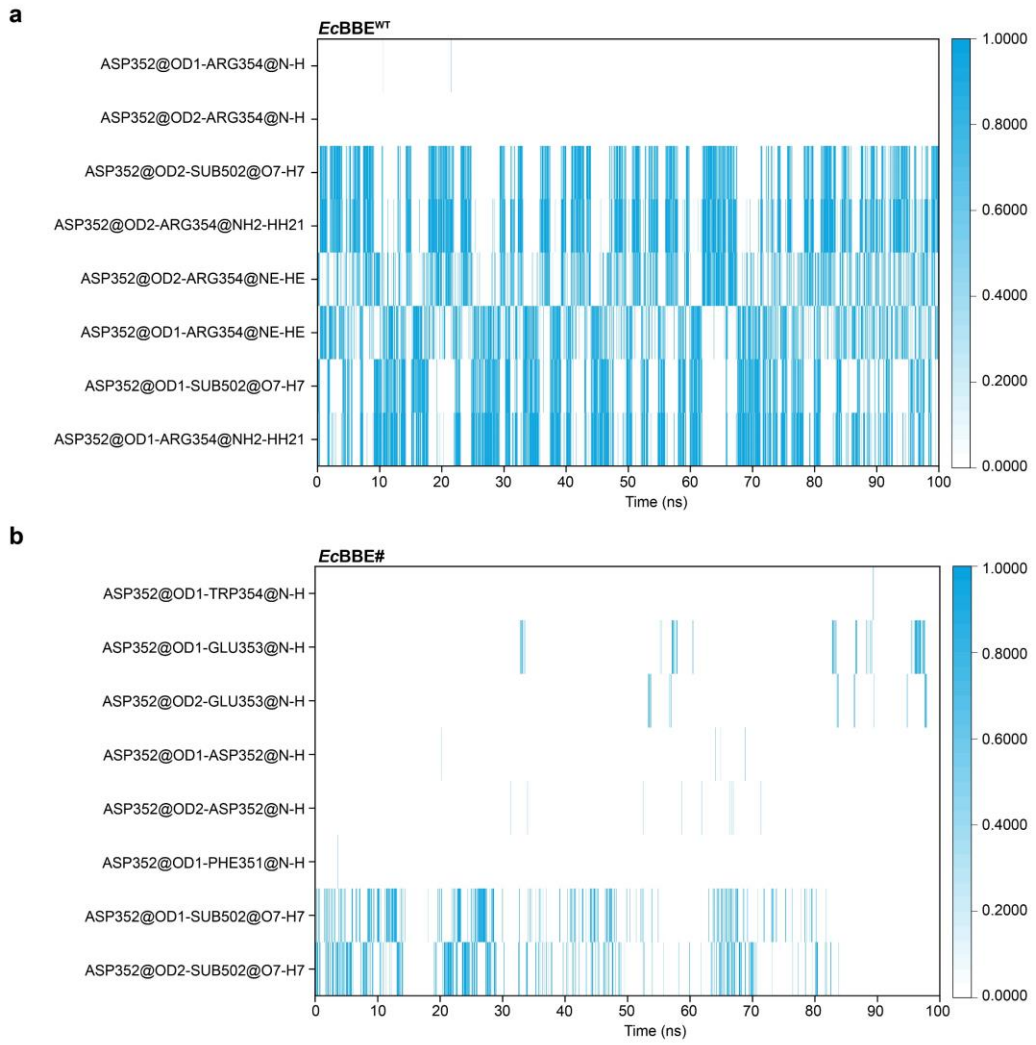

Supplementary Figure 24. Heat map of hydrogen-bond interactions between (*S*)-5a and *Ec*BBE in MD simulations. a Heat map of hydrogen-bond interactions between (*S*)-**5a** and *Ec*BBE^{WT}. **b** Heat map of hydrogen-bond interactions between (*S*)-**5a** and *Ec*BBE#. Source data are provided as a Source Data file.

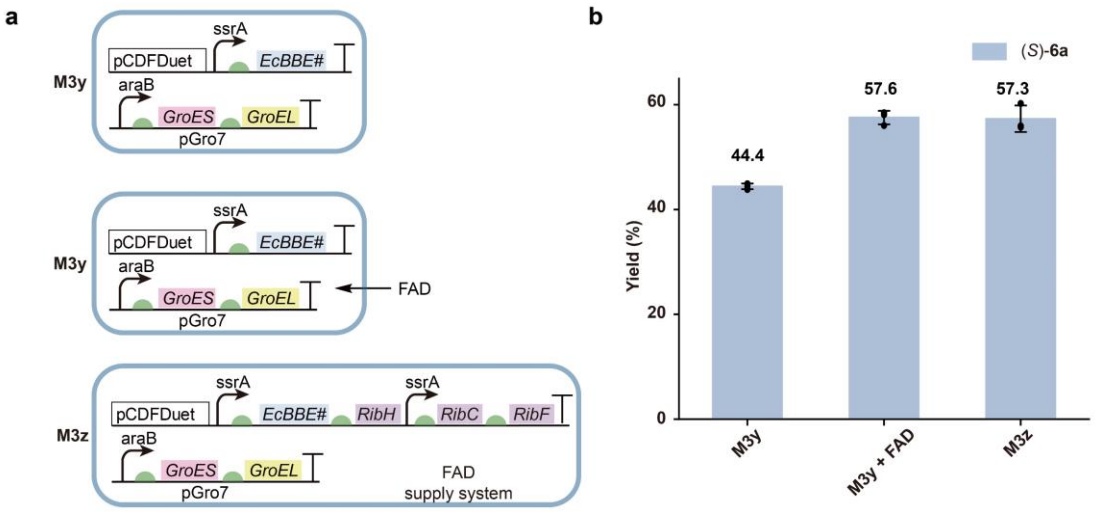

Supplementary Figure 25. Optimization of FAD exogenous addition and the FAD supply system to improve the yield of (*S*)-6a. a Scheme of the designed biosynthetic pathway to produce (*S*)-**6a** by adding FAD exogenously in strain M3y or by introducing the FAD supply system in strain M3z. **b** Yields of (*S*)-**6a** correspond to a theoretical yield of **1a** in strain M3y, strain M3y with FAD adding exogenously and strain M3z. All data is presented as mean value of three independent experiments and the error bars indicate ± sd. Source data are provided as a Source Data file.

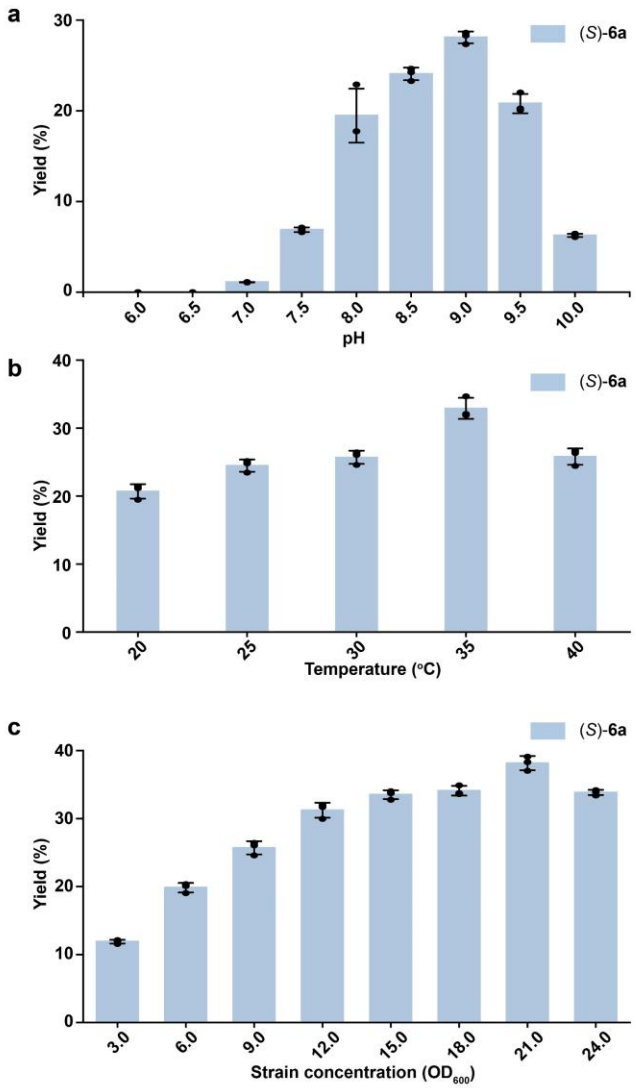

Supplementary Figure 26. Optimization of the parameters to improve the yield of (*S*)-6a correspond to a theoretical yield of 1a in the BBE module. a Optimization of the reaction pH in the BBE module by strain M3z. **b** Optimization of the reaction temperature in the BBE module by strain M3z. **c** Optimization of the concentration of the strain M3z in the BBE module. All data is presented as mean value of three independent experiments and the error bars indicate ± sd. Source data are provided as a Source Data file.

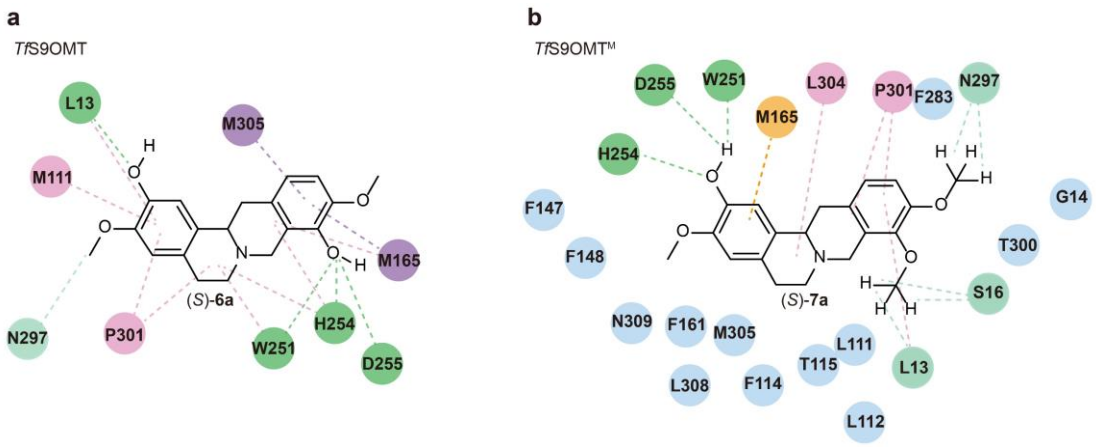

Supplementary Figure 27. Two-dimensional docking diagram and molecular interactions of (*S*)-6a with *Tf*S9OMT and (*S*)-7a with *Tf*S9OMT^{M}. a Two-dimensional docking diagram and molecular interactions of (*S*)-**6a** with *Tf*S9OMT. **b** Two-dimensional docking diagram and molecular interactions of (*S*)-**7a** with *Tf*S9OMT^{M}. Van der Waals: light blue, conventional hydrogen bond: green, carbon hydrogen bond: cyan, π-sulfur: orange, π-alkyl: pink, π-sigma: purple.

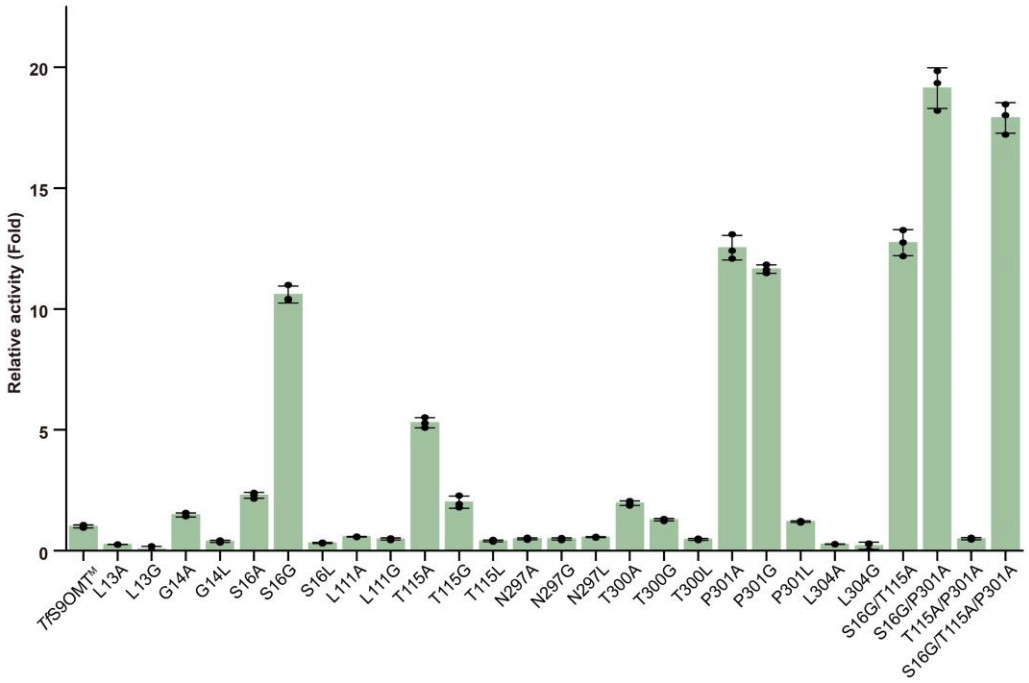

Supplementary Figure 28. Relative activity of all mutants of *Tf*S9OMT^{M} toward (*S*)-6a *in vitro*. The relative activity is defined as the ratio of the Rotundine titer of *Tf*S9OMT^{M} mutants to that of *Tf*S9OMT^{M}. All data is presented as mean value of three independent experiments and the error bars indicate ± sd. Source data are provided as a Source Data file.

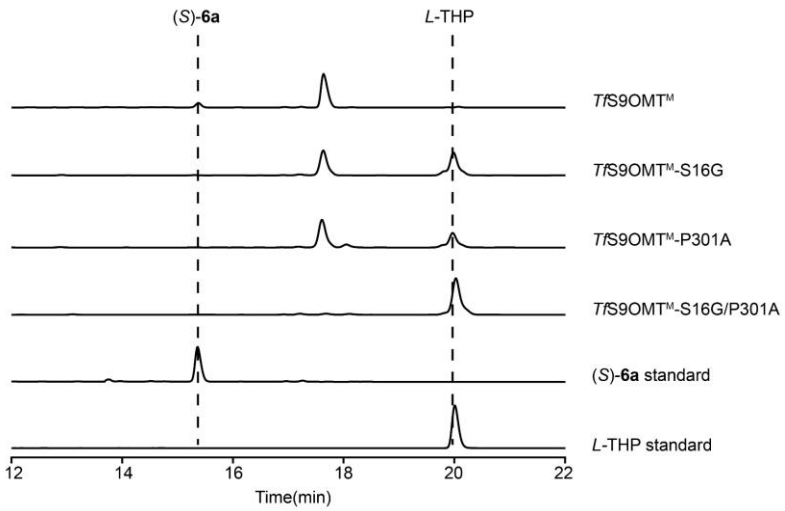

Supplementary Figure 29. HPLC analysis of *Tf*S9OMT^{M} and its mutants. Source data are provided as a Source Data file.

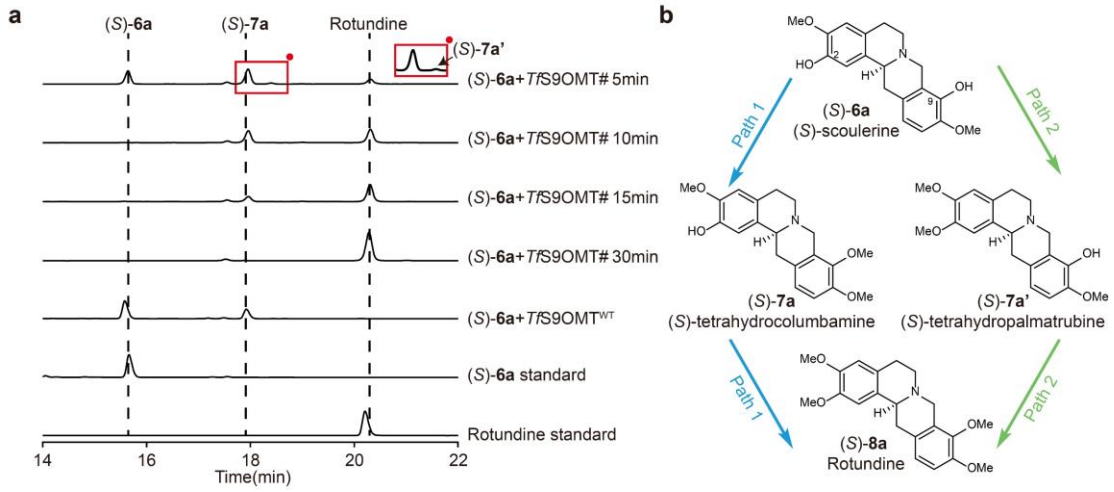

Supplementary Figure 30. Potential catalytic pathways study of *Tf*S9OMT#. a HPLC analysis *in vitro* assays of *Tf*S9OMT#. The new product (postulated as (*S*)-**7a'**) was observed when enlarging the spectrum highlighted in red rectangle. **b** Two putative paths of Rotundine synthesis by *Tf*S9OMT#. Pathway 1 highlighted in blue involves the methylation first occurs at 9-hydroxyl position before the 2-position. Pathway 2 highlighted in green involves the methylation first occurs at 2-hydroxyl position before the 9-position. Source data are provided as a Source Data file.

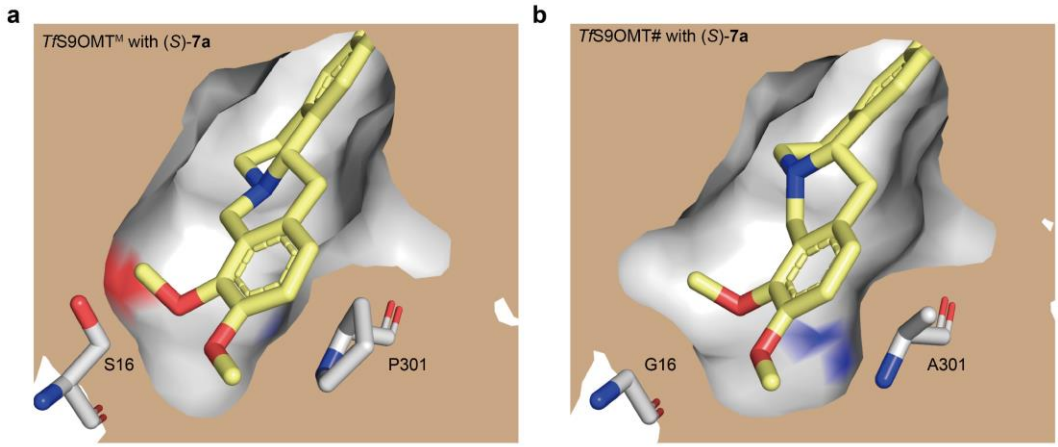

Supplementary Figure 31. Cross-section of the substrate binding pocket of *Tf*S9OMT. a Substrate binding site highlighted in cross-section of *Tf*S9OMT^{M}. **b** Substrate binding site highlighted in cross-section of *Tf*S9OMT#.

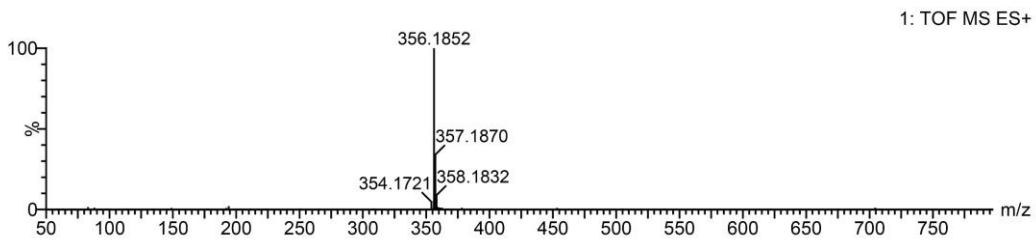

Supplementary Figure 32. HRMS spectrum of Rotundine ((*S*)-8a). The HRMS spectrum (positive) showed *m/z* 356.1852 for $[M+H]^+$ (calcd. for $C_{21}H_{25}NO_4^+$, 356.1856).

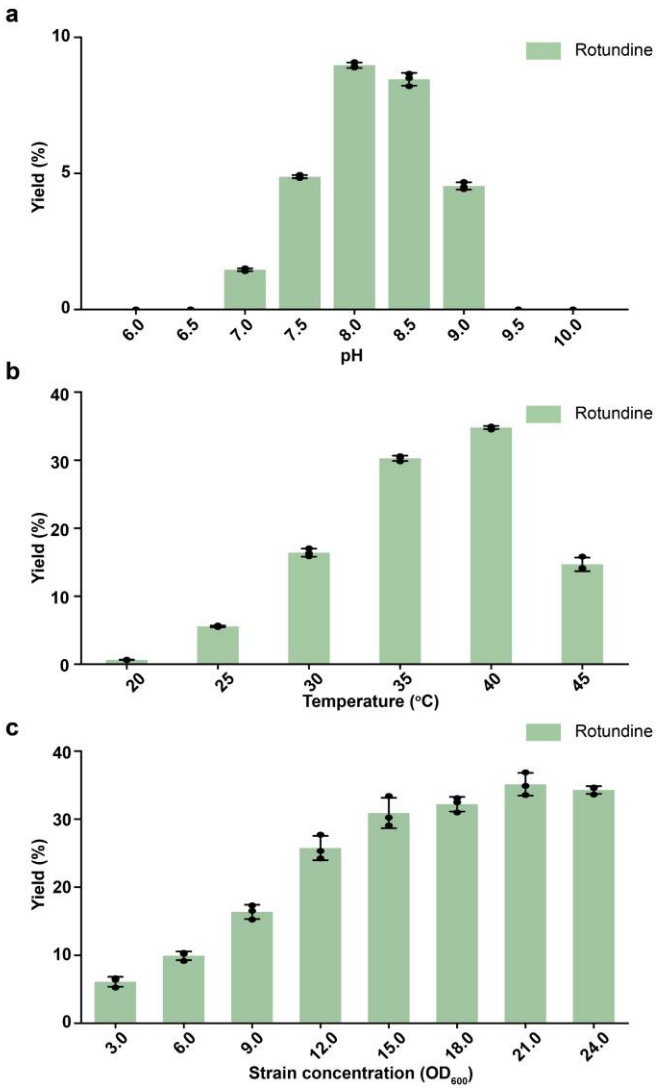

Supplementary Figure 33. Optimization of the parameters to improve the yield of Rotundine correspond to a theoretical yield of 1a in the S9OMT module. a Optimization of the reaction pH in the S9OMT module by strain M4b. **b** Optimization of the reaction temperature in the S9OMT module by strain M4b. **c** Optimization of the concentration of the strain M4b in the S9OMT module. All data is presented as mean value of three independent experiments and the error bars indicate ± sd. Source data are provided as a Source Data file.

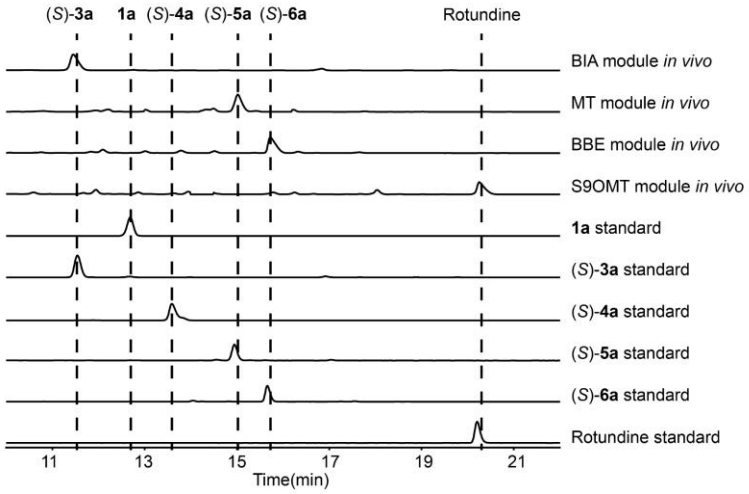

Supplementary Figure 34. Establishment of a multi-enzyme cascade reaction to efficiently synthesize Rotundine *in vivo*. Source data are provided as a Source Data file.

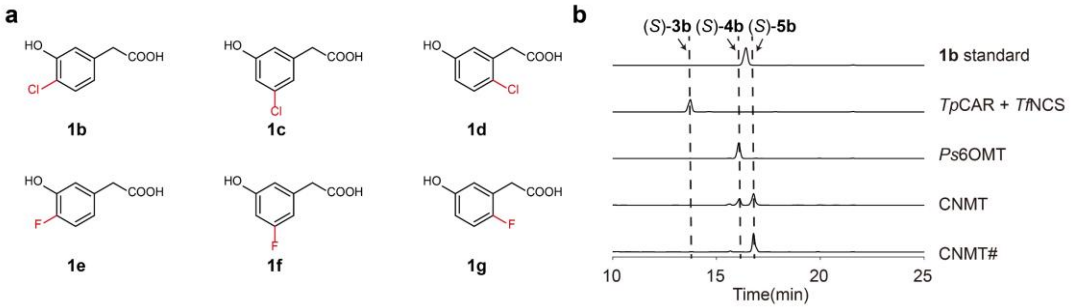

Supplementary Figure 35. a Structures of halogenated substrates. **b** HPLC analysis of reactions of **1b** *in vitro*, dotted line: predicted intermediates and products. Source data are provided as a Source Data file.

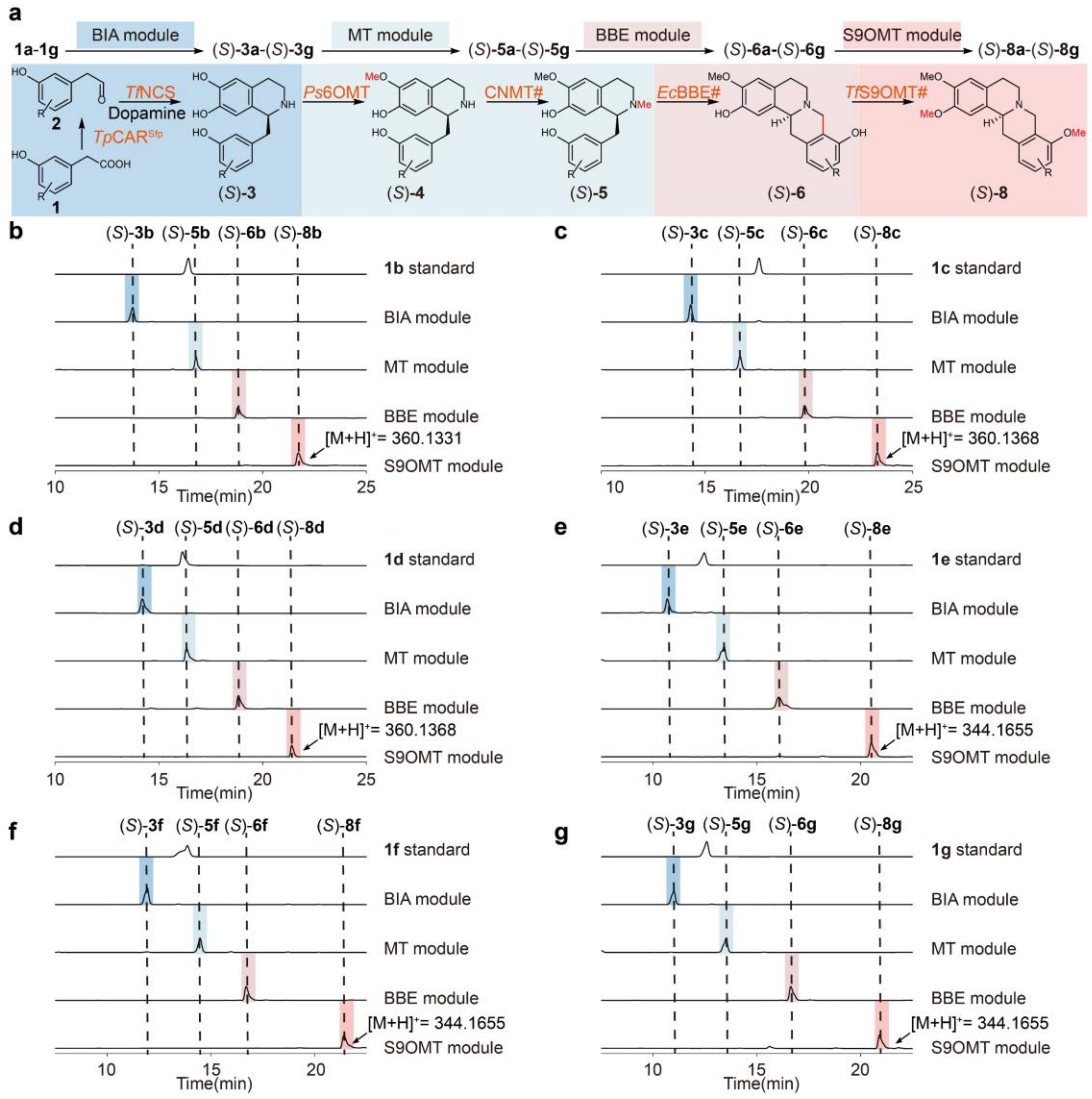

Supplementary Figure 36. HPLC analysis of reactions of halogenated substrates *in vitro* through the designed enzyme cascade. a Biosynthesis of various halogenated protoberberine alkaloids by the optimized six-enzyme cascade. **b** HPLC analysis of the cascade reactions of **1b**, with the HRMS result of the desired product (*S*)-**8b**. **c** HPLC analysis of the cascade reactions of **1c**, with the HRMS result of the desired product (*S*)-**8c**. **d** HPLC analysis of the cascade reactions of **1d**, with the HRMS result of the desired product (*S*)-**8d**. **e** HPLC analysis of the cascade reactions of **1e**, with the HRMS result of the desired product (*S*)-**8e**. **f** HPLC analysis of the cascade reactions of **1f**, with the HRMS result of the desired product (*S*)-**8f**. **g** HPLC analysis of the cascade reactions of **1g**, with the HRMS result of the desired product (*S*)-**8g**. Blue square: new peak in the BIA module; light blue square: new peak in the MT module; light powder square: new peak in the BBE module; pink square: new peak in the S9OMT module; dotted line: predicted intermediates and products. Source data are provided as a Source Data file.

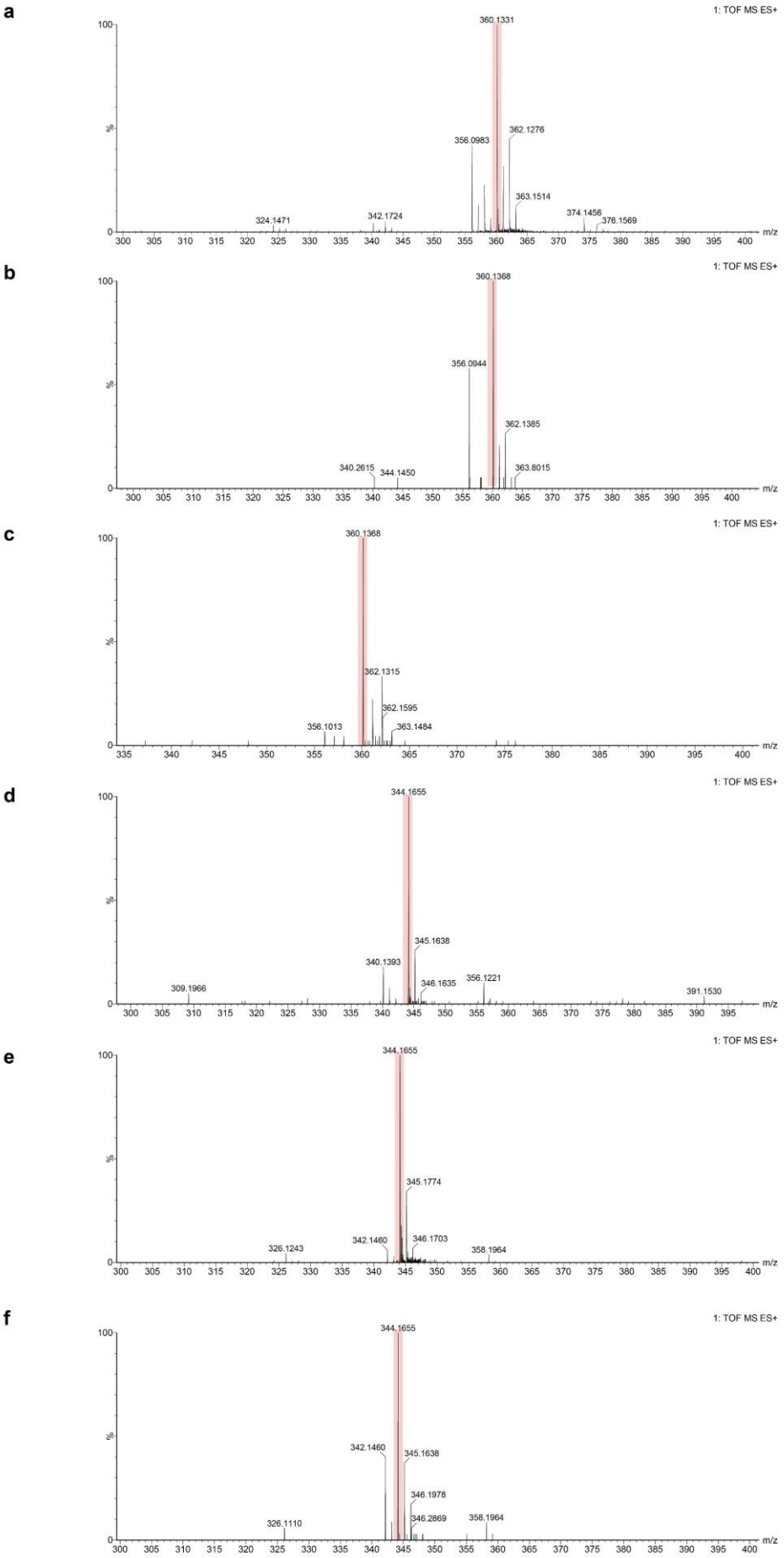
a
1: TOF MS ES+
360.1331
356.0983
362.1276
363.1514
324.1471
342.1724
374.1456
376.1569
b
1: TOF MS ES+
360.1368
356.0944
362.1385
340.2615
344.1450
363.8015
c
1: TOF MS ES+
360.1368
362.1315
362.1595
356.1013
363.1484
d
1: TOF MS ES+
344.1655
345.1638
340.1393
346.1635
356.1221
309.1966
391.1530
e
1: TOF MS ES+
344.1655
345.1774
342.1460
346.1703
326.1243
358.1964
f
1: TOF MS ES+
344.1655
342.1460
345.1638
346.1978
346.2869
326.1110
358.1964
m/z

Supplementary Figure 37. HRMS spectrum of halogenated protoberberine alkaloids. a HRMS spectrum (positive) showed *m/z* 360.1331 for $[M+H]^+$ (calcd. for $C_{20}H_{22}ClNO_3^+$, 360.1361) of (*S*)-**8b**. **b** HRMS spectrum (positive) showed *m/z* 360.1368 for $[M+H]^+$ (calcd. for $C_{20}H_{22}ClNO_3^+$, 360.1361) of (*S*)-**8c**. **c** HRMS spectrum (positive) showed *m/z* 360.1368 for $[M+H]^+$ (calcd. for $C_{20}H_{22}ClNO_3^+$, 360.1361) of (*S*)-**8d**. **d** HRMS spectrum (positive) showed *m/z* 344.1655 for $[M+H]^+$ (calcd. for $C_{20}H_{22}FNO_3^+$, 344.1656) of (*S*)-**8e**. **e** HRMS spectrum (positive) showed *m/z* 344.1655 for $[M+H]^+$ (calcd. for $C_{20}H_{22}FNO_3^+$, 344.1656) of (*S*)-**8f**. **f** HRMS spectrum (positive) showed *m/z* 344.1656 for $[M+H]^+$ (calcd. for $C_{20}H_{22}FNO_3^+$, 344.1655) of (*S*)-**8g**.

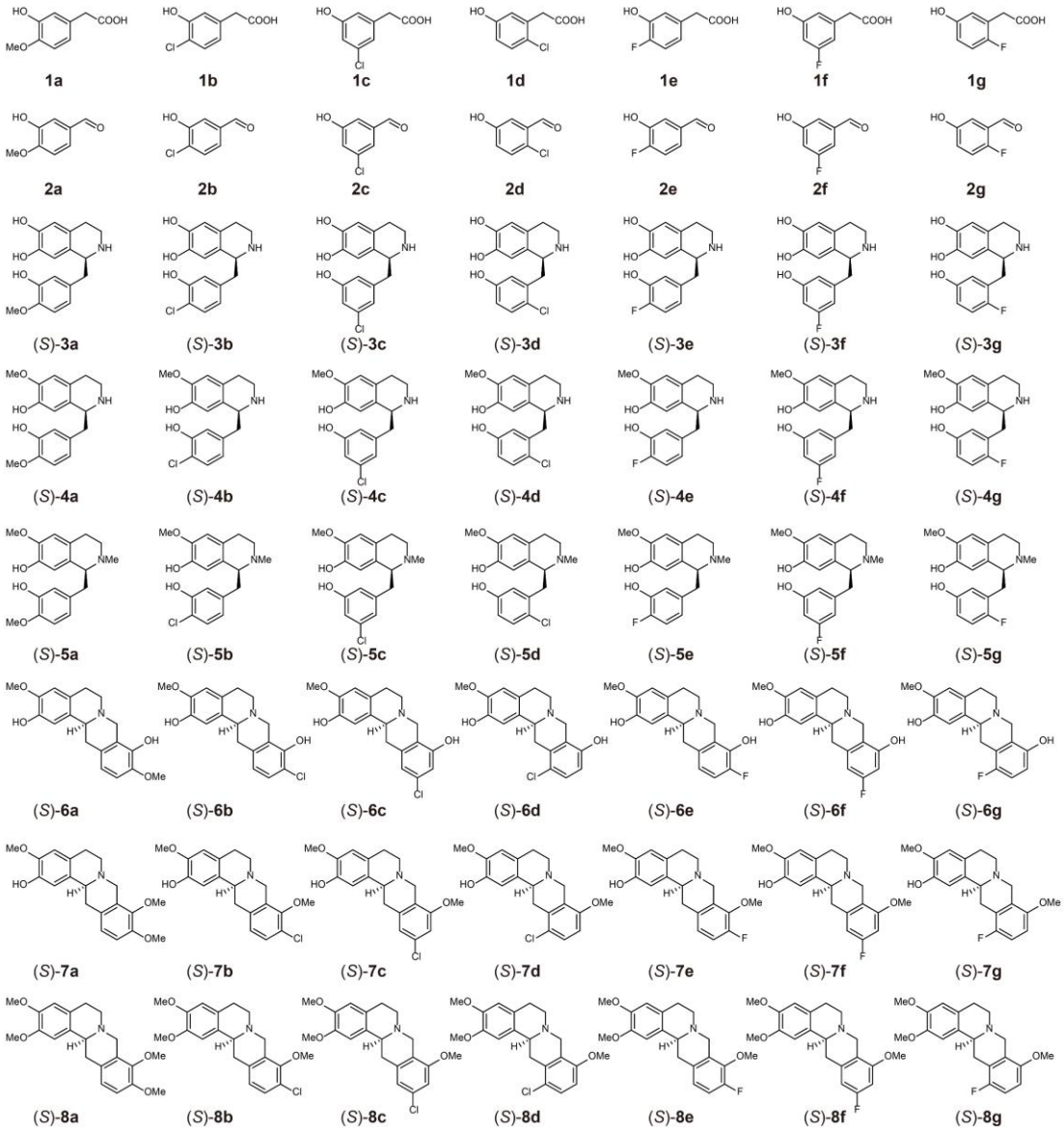

Supplementary Figure 38. Structures of substrates and all the identified and predicted intermediates in this research.

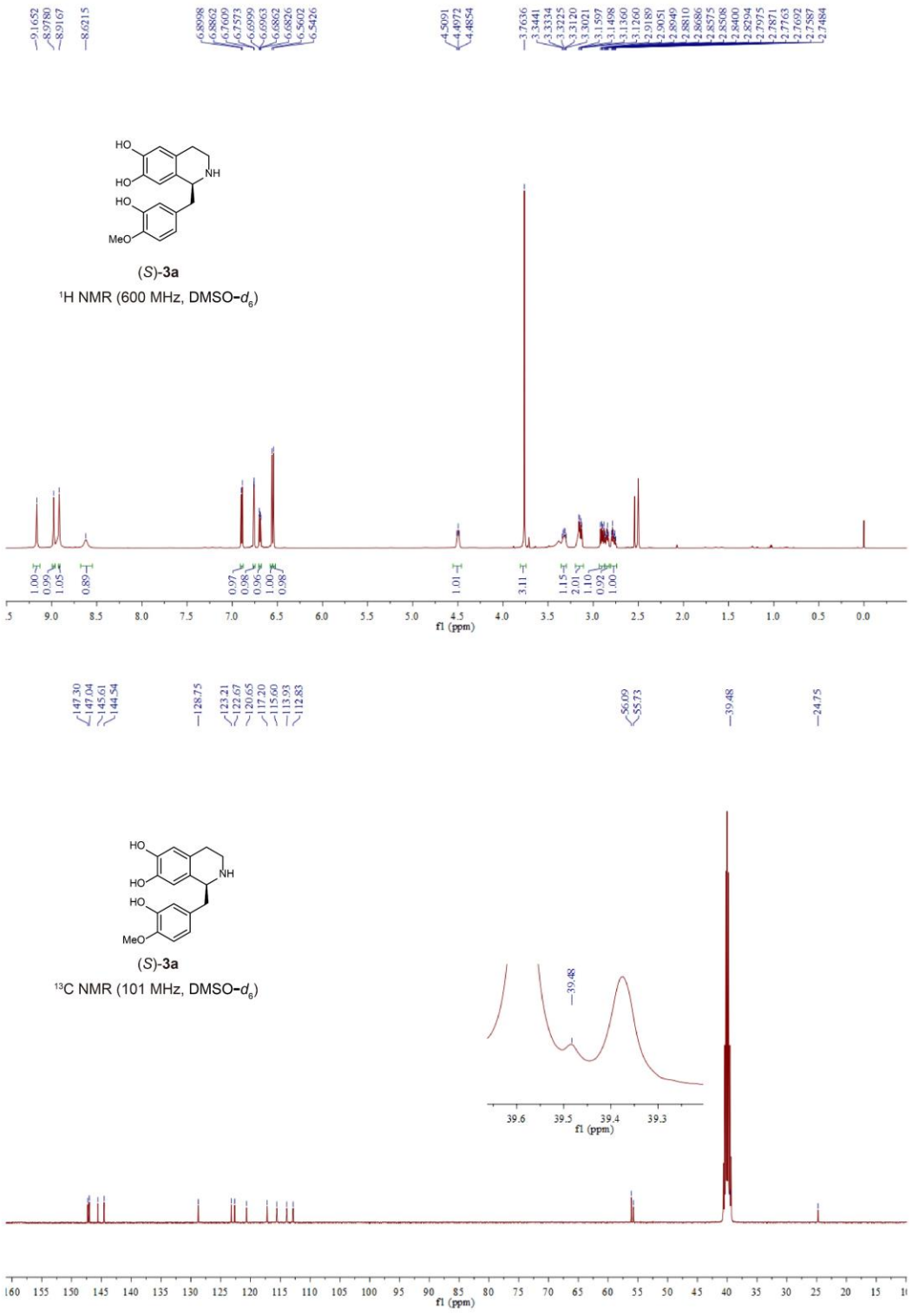

Supplementary Figure 39. ^{1}H NMR and ^{13}C NMR spectra of (*S*)-3a.

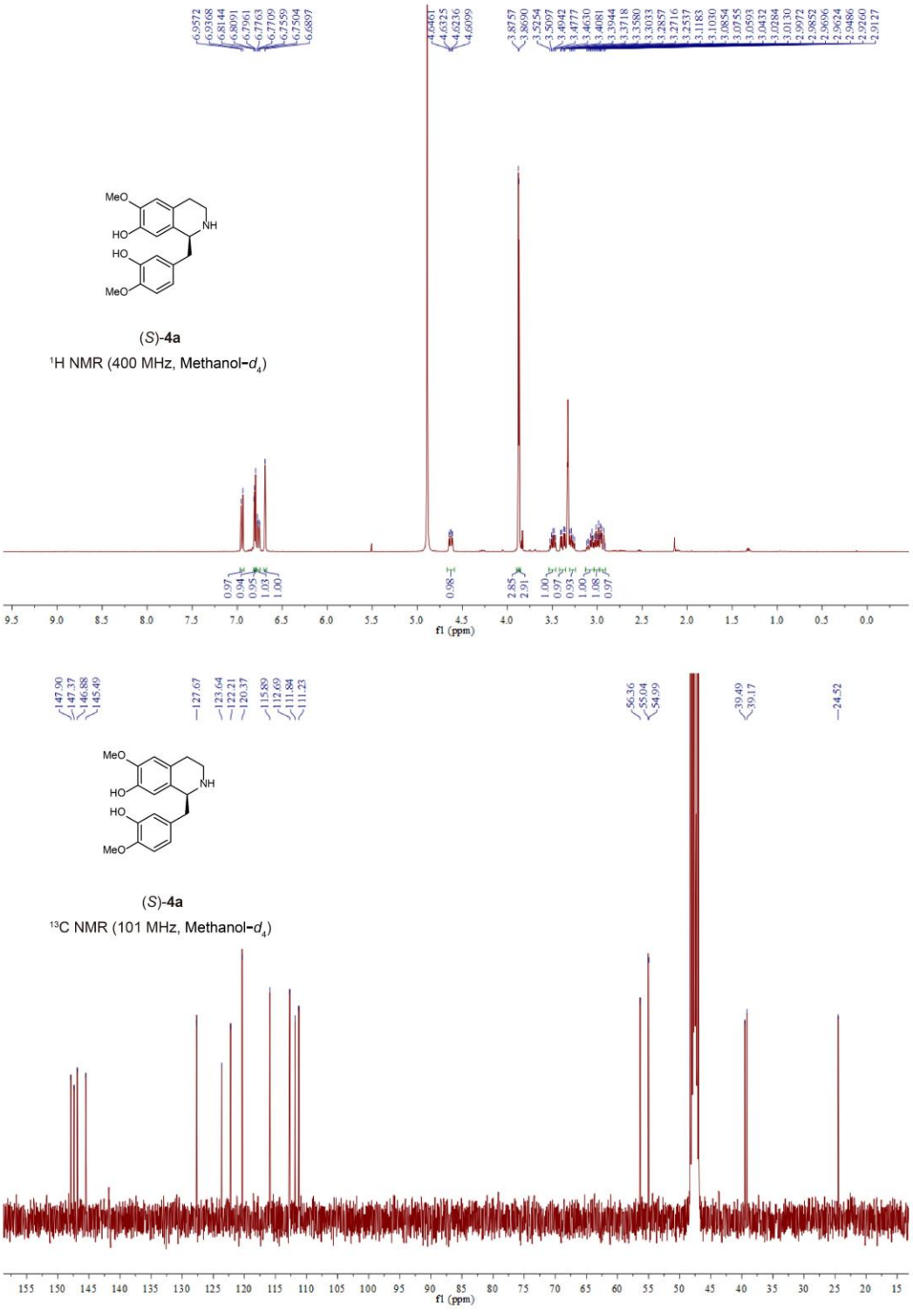

Supplementary Figure 40. ^{1}H NMR and ^{13}C NMR spectra of (*S*)-4a.

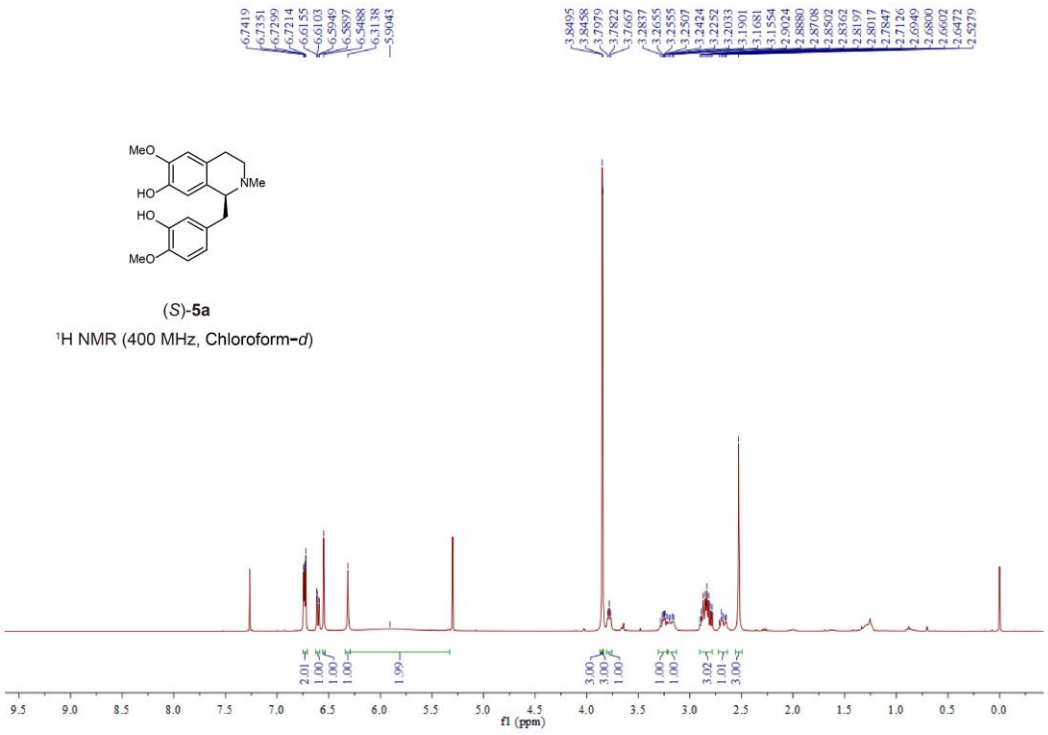

Supplementary Figure 41. ^{1}H NMR spectrum of (*S*)-5a.

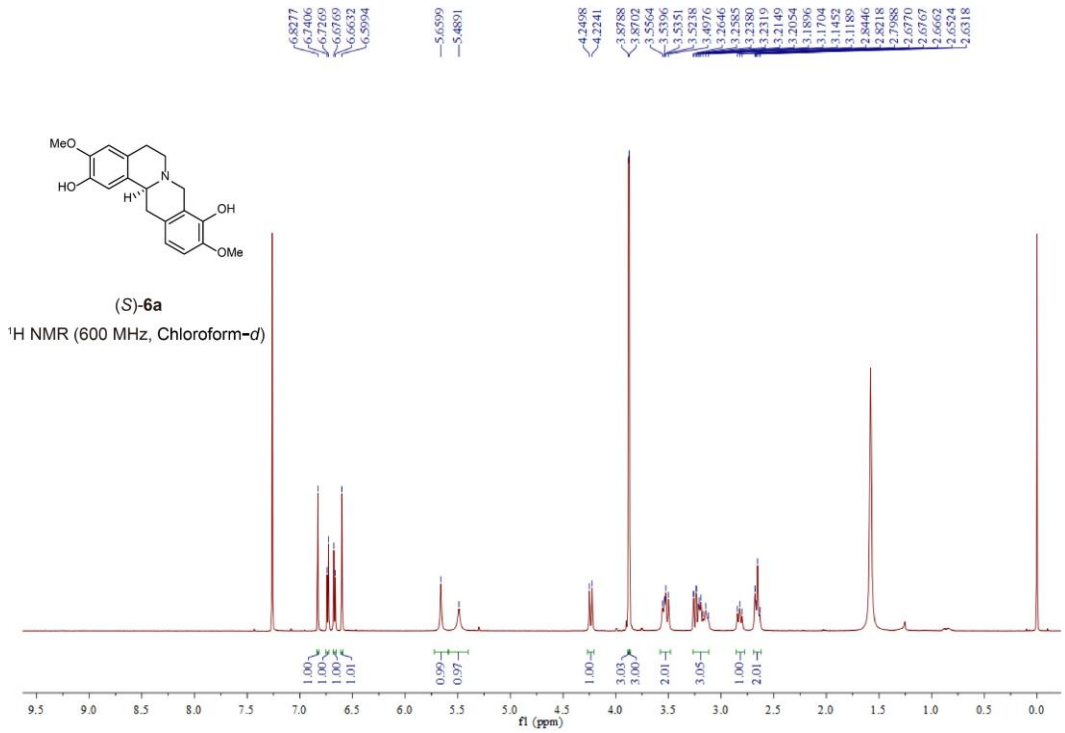

Supplementary Figure 42. ^{1}H NMR spectrum of (*S*)-6a.

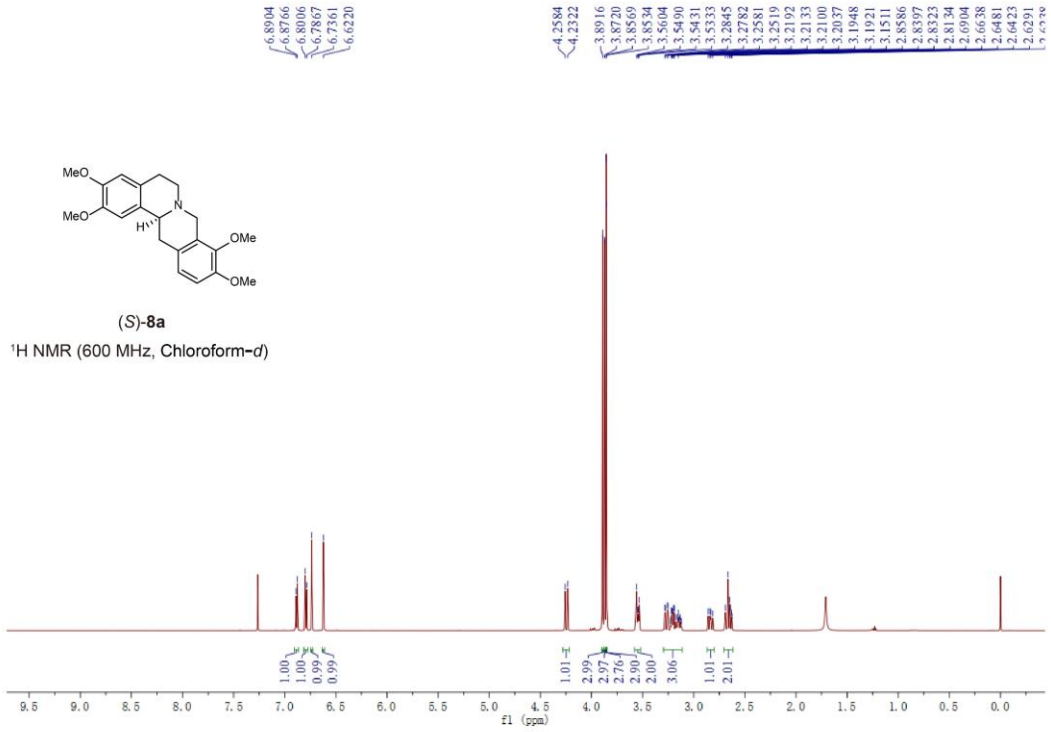

Supplementary Figure 43. ^{1}H NMR spectrum of (*S*)-8a.

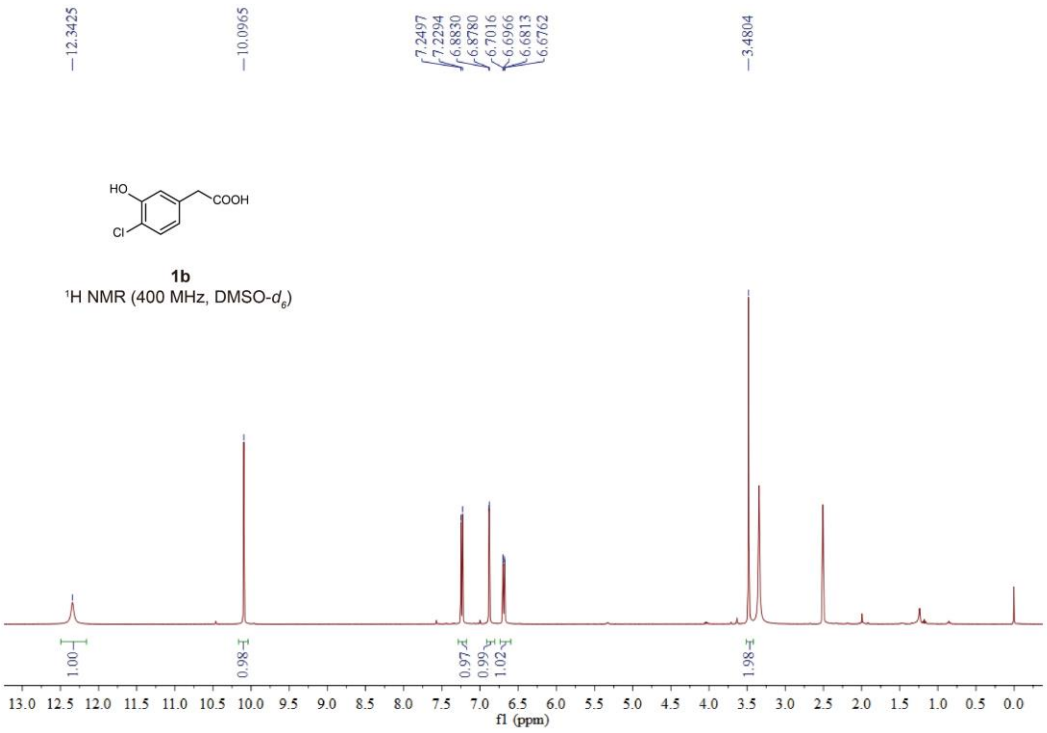

Supplementary Figure 44. ^{1}H NMR spectrum of 1b.

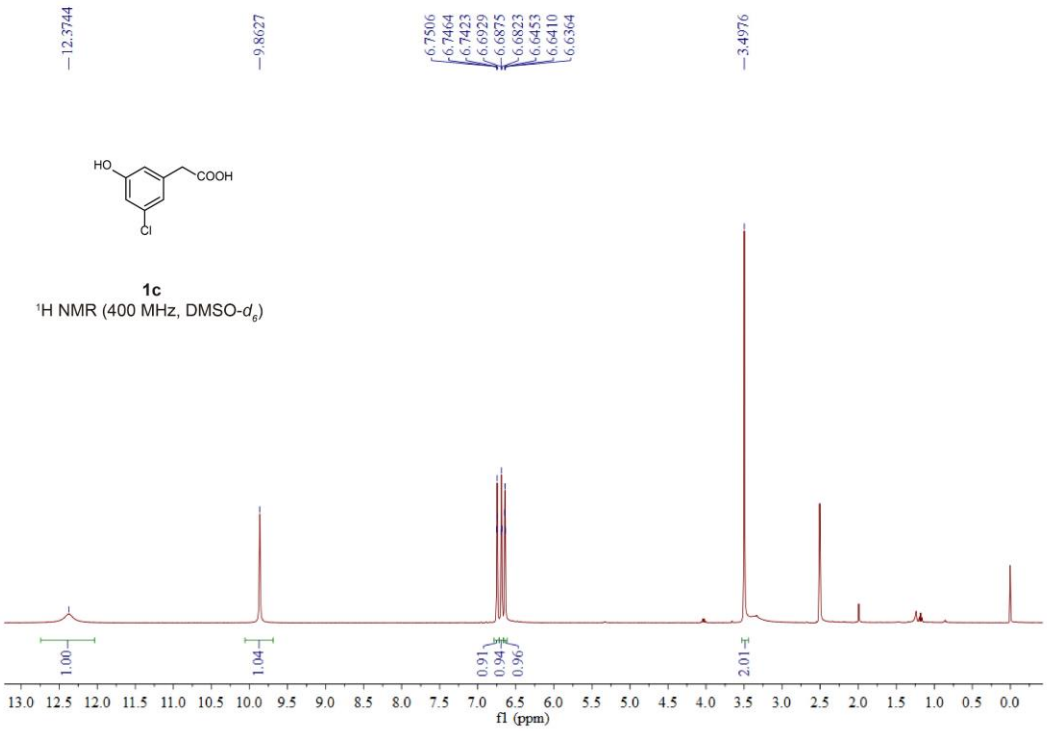

Supplementary Figure 45. ^{1}H NMR spectrum of 1c.

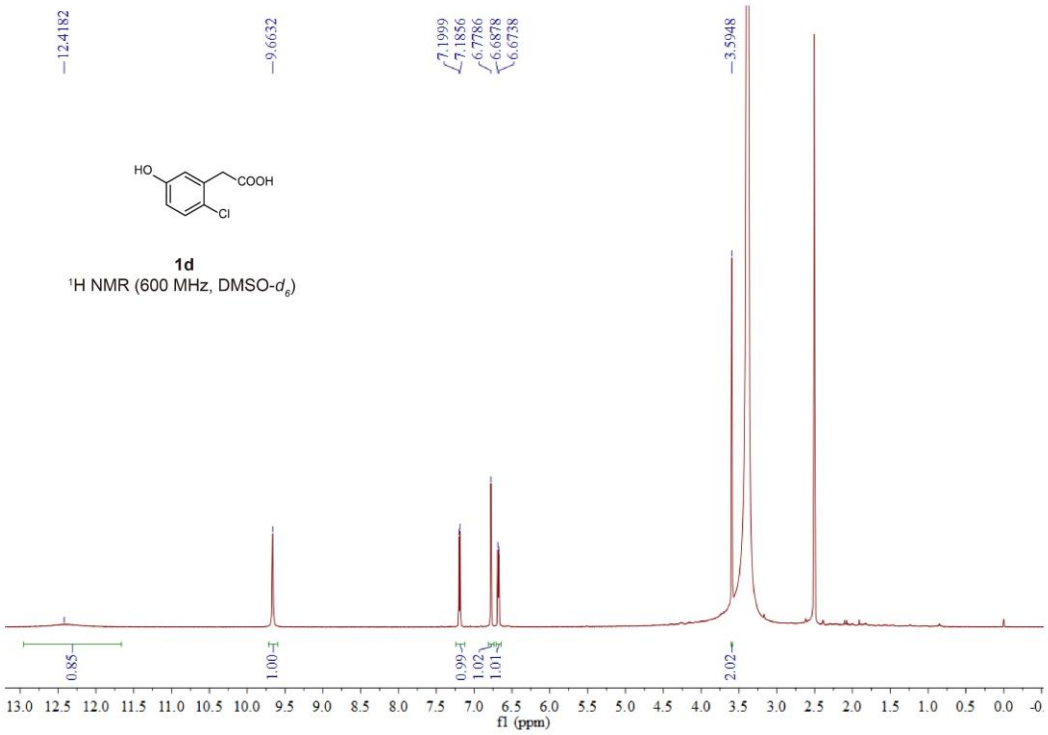

Supplementary Figure 46. ^{1}H NMR spectrum of 1d.

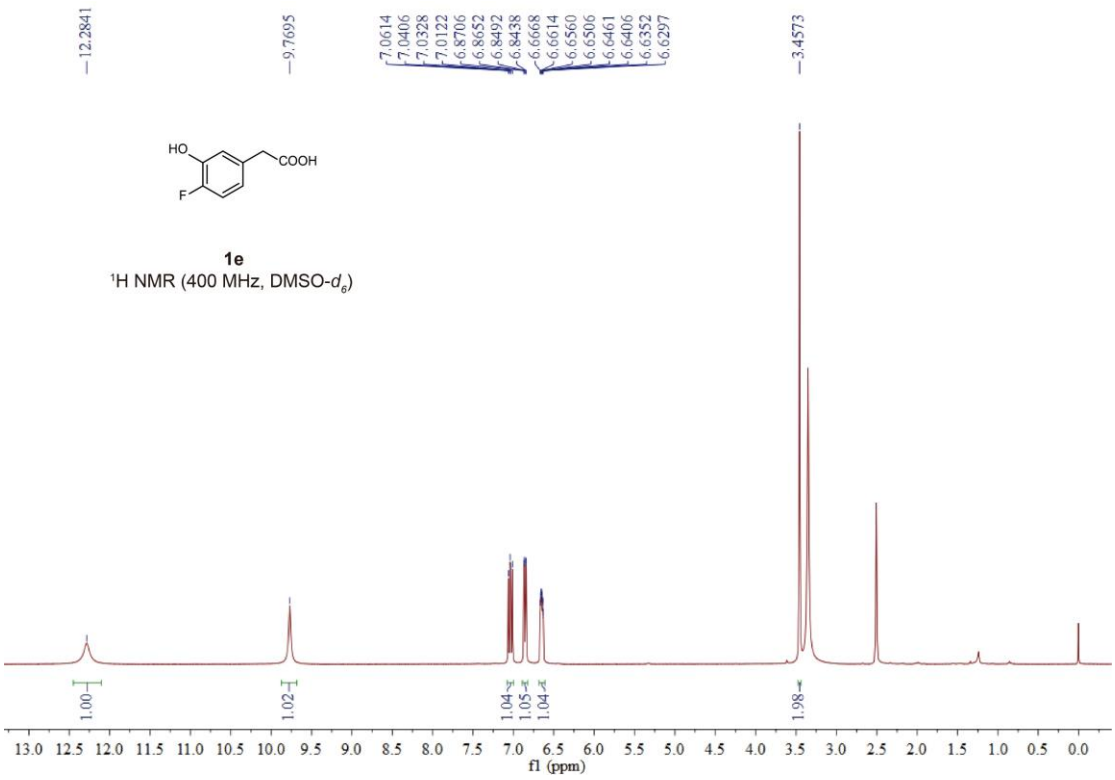

Supplementary Figure 47. ^{1}H NMR spectrum of 1e.

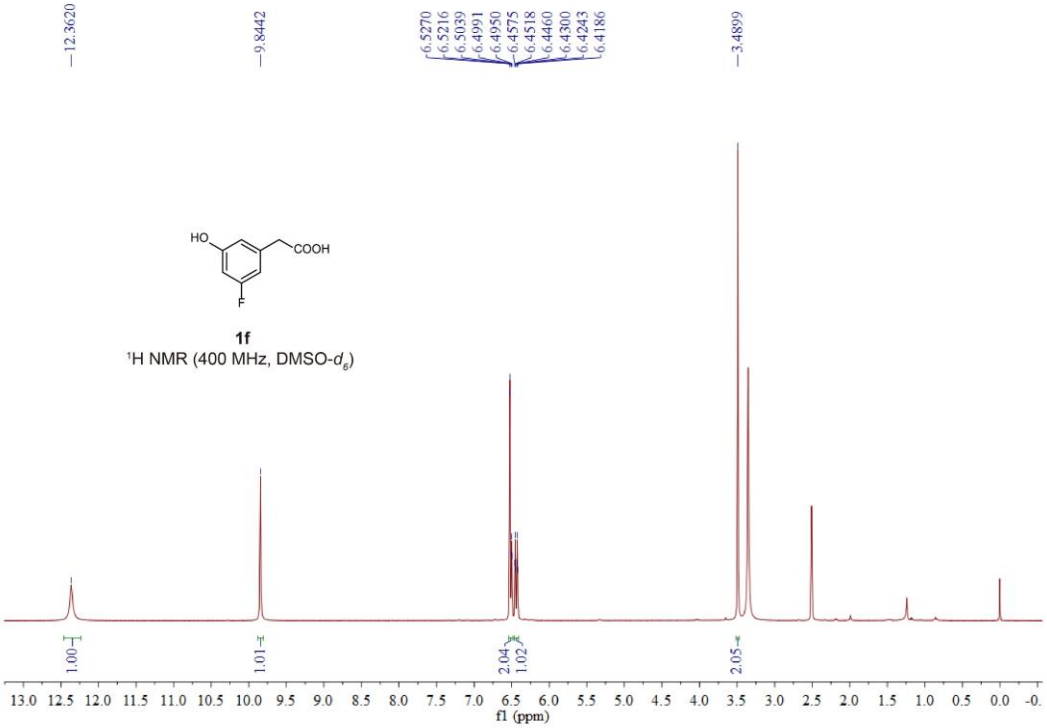

Supplementary Figure 48. ^{1}H NMR spectrum of 1f.

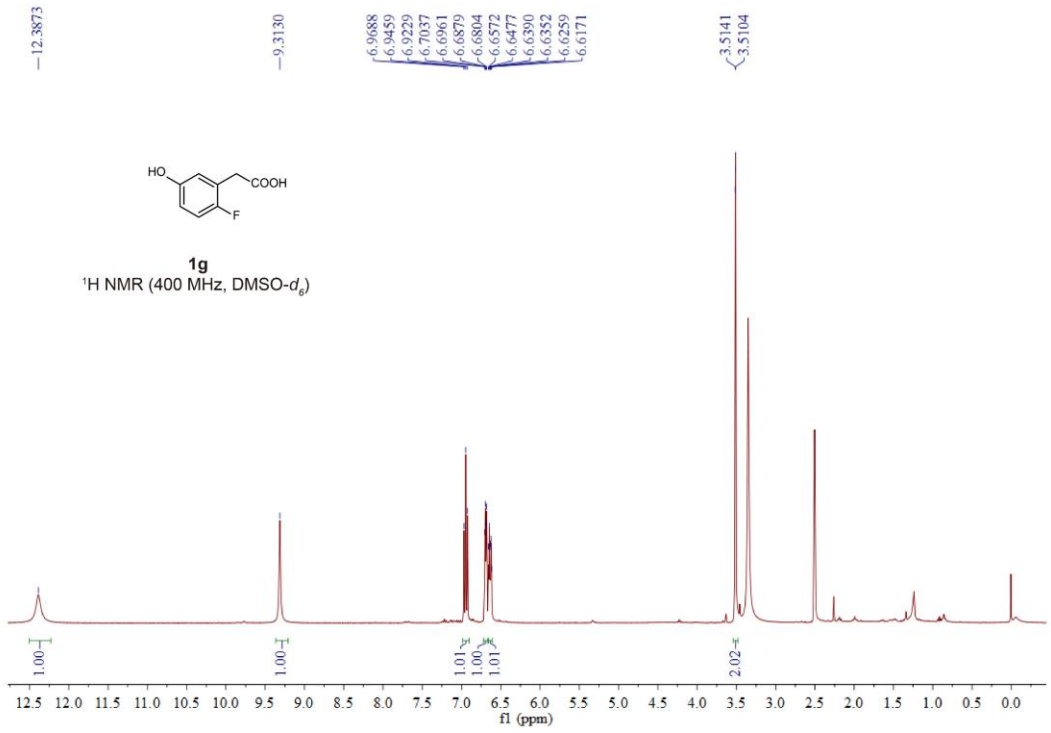

Supplementary Figure 49. ^{1}H NMR spectrum of 1g.

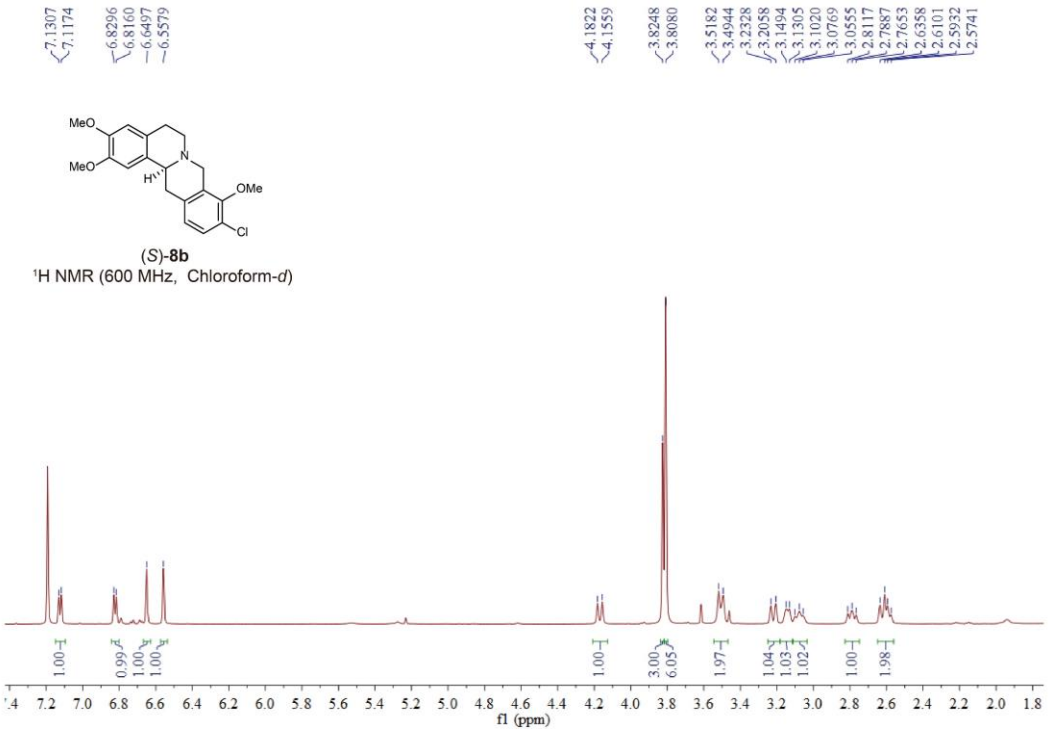

Supplementary Figure 50. ^{1}H NMR spectra of (*S*)-8b.

Supplementary reference

1. Schrittwieser, J. H. *et al.* Deracemisation of benzylisoquinoline alkaloids employing monoamine oxidase variants. *Catal. Sci. Technol.* **4**, 3657-3664 (2014).
2. Schrittwieser, J. H. *et al.* Biocatalytic organic synthesis of optically pure (*S*)-scoulerine and berbine and benzylisoquinoline alkaloids. *J. Org. Chem.* **76**, 6703-6714 (2011).
3. Li, W. J. *et al.* Total synthesis of (-)-canadine, (-)-rotundine, (-)-sinactine, and (-)-xylopinine using a last-step enantioselective Ir-catalyzed hydrogenation. *J. Org. Chem.* **86**, 8143-8153 (2021).